

Static and dynamic interaction of superconducting vortices with a periodic pinning potential*

Piero Martinoli

*Laboratorium für Festkörperphysik, Eidgenössische Technische Hochschule, Zürich, CH-8093 Zürich, Switzerland
and Ames Laboratory-ERDA and Department of Physics, Iowa State University, Ames, Iowa 50011*

(Received 15 August 1977)

A model is developed which describes the static and dynamic interaction of the vortex lattice with the pinning potential due to harmonic one-dimensional variations of the thickness of superconducting films. Using a London-Pearl approach, an expression is derived for the free energy of the mixed state in thin modulated films from which static equilibrium configurations of the vortex lattice and the corresponding deformations due to the harmonic pinning force are deduced. Lattice configurations of lowest energy are found when the magnetic induction B corresponds to matching of the (undistorted) triangular vortex lattice to the periodic pinning structure. Particular attention is devoted to lattice configurations slightly deviating from a matching situation, for which long-wavelength transverse deformations are found predominant, and to Bragg configurations, where short-wavelength deformations of wave vector $\vec{k} = (1/2)\vec{g}_1$ (\vec{g}_1 is a nearest-neighbor reciprocal lattice vector) propagate along a high-symmetry direction of the triangular lattice. We estimate the critical current density, $j_c(B)$, for these lattice configurations. A matching peak in the $j_c(B)$ -curve is found to have approximately a resonantlike shape whose width depends on the shear modulus of the lattice and on the strength of the elementary interaction of a single flux line with the pinning potential. The flux-flow regime is also investigated when steady-state vortex motion results from the equilibrium of the Lorentz driving force, the viscous damping force, the harmonic pinning force, and the pinning-induced lattice restoring force. A highly coherent flux-flow regime with rf properties similar to those of series arrays of resistively shunted Josephson junctions acting in phase and frequency coherence (super-radiant state) is found in the dynamic matching state. For nonmatching configurations we study the influence of dynamically excited lattice deformation modes on the current-voltage characteristics when vortex motion is driven by dc or by superimposed dc and rf transport currents. In particular, for nearly matching configurations the width of the rf-induced interference transitions is related to the shear modulus of the vortex lattice and to the flux-flow resistivity.

I. INTRODUCTION

It is well known that the transport properties of inhomogeneous (or nonideal) type II superconductors depend strongly on the interaction of vortex lines with pinning centers.¹ In this connection a basic problem of great technological importance is undoubtedly the calculation of their critical currents as a function of magnetic field, temperature, and pinning configuration. This is, however, an exceedingly difficult task because of the complexity, variety, and spatial distribution of the pinning structures involved. For this reason, considerable interest has recently been devoted to the interaction of the quantized vortex lattice with well-defined periodic pinning structures.²⁻⁸ Such regular pinning configurations offer the unique and attractive possibility of comparing critical currents deduced from experiments with theoretical estimates based on simple models.

So far, two kinds of periodic pinning structures have been investigated. In the experiments of Raffy *et al.*,^{2,4,5} a periodic pinning configuration was achieved by spatially modulating the impurity (Bi) concentration of superconducting Pb/Bi alloy films along their thickness. In this case, the pinning mechanism is related to periodic changes of the

two parameters characterizing the mixed state: the penetration depth $\lambda(T)$ and the coherence length $\xi(T)$, both depending in opposite ways on the electronic mean free path. As a consequence, the energy of a vortex line also becomes a periodic function of position showing minima in regions of higher impurity concentration for materials characterized by large κ values (κ is the Ginzburg-Landau parameter). Therefore, these regions act as pinning planes for the vortex lattice created by a magnetic field parallel to the films. The second type of controlled pinning structure is that considered by Martinoli *et al.*,^{3,6-8} who studied the static and dynamic (flux-flow) behavior of the vortex lattice in superconducting granular Al films with periodically modulated thickness placed in a transverse magnetic field. In a simple picture, neglecting to a first approximation the thickness dependence of λ and ξ in very thin films, the vortex line energy is proportional to its length. This suggests that in these experiments the thickness minima should play the role of pinning lines.

An interesting feature of these periodic film structures is the presence of characteristic peaks in the critical current density (j_c) versus magnetic field (H) curves. The j_c maxima appear at well-defined field values corresponding to matching of

the flux-line lattice to the periodic pinning array. At a matching field the lowest energy configuration of the vortex lattice is achieved by flux lines localized at the pinning sites described above. Since in this situation each flux line simultaneously experiences the pinning effect of the periodic structure, one expects the pinning force, and therefore j_c , to reach a maximum value. This behavior, on the other hand, suggests that a matching configuration corresponds to "resonant" coupling of the vortex lattice with the periodic potential induced by the pinning structure.

An interesting and spectacular aspect of periodic pinning structures is, however, that observed by us^{7,8} in experiments on the dynamic interaction of the vortex lattice with the periodic pinning potential in thickness-modulated films. Inspired by a previous paper of Fiory⁹ we investigated modulated films in the flux-flow regime driven by superimposed dc and radio frequency (rf) transport currents. For a matching configuration we observed pronounced supercurrent steps in the current-voltage I-V characteristics.⁷ These steps are a manifestation of a Josephson-like ac quantum interference effect and appear at voltages for which the characteristic frequency associated with vortex motion in the periodic potential is a multiple of that of the applied rf field.

The pinning potential plays a crucial role in these flux-flow experiments. In fact, it introduces the necessary mechanism¹⁰ for coupling the electromagnetic field to the supercurrent oscillations generated by vortex motion in the flux-flow regime. As pointed out by Meincke,¹¹ this is almost excluded in ideal type II superconductors. This coupling, however, is possible when the effect of pinning results in a sufficiently coherent modulation of the vortex velocity as in the case of a matching configuration. For this particular situation the corresponding modulation of the oscillating supercurrent density distribution leads to a net supercurrent oscillation whose interaction with an applied rf field gives rise to the interference transitions observed in the I-V characteristics. Direct experimental evidence for the existence of the superfluid quantum oscillation generated by the moving vortex lattice has been recently provided by Martinoli *et al.*⁸ who detected the rf voltages arising from the oscillation in the dissipative flux-flow regime.

The static interaction of the vortex lattice with the periodic pinning structure achieved by Raffy *et al.* has been studied theoretically by Ami and Maki¹² and by Dobrosavljević.¹³ On the other hand, there is no theoretical model treating the static and dynamic behavior of superconducting vortices in thickness-modulated films. It is the purpose of

the present work to develop a model for this particular experimental situation. Our approach is based on the London model of the mixed state¹⁴ which is known to be valid for extreme type II materials and at moderate flux-line densities ($B \ll H_{c2}$). We restrict our considerations to very thin films and assume that the radial vortex size is much less than the typical scale of the pinning structure (local approximation). Furthermore, only the case of weakly modulated layers is discussed.

In Sec. II, we discuss the static interaction of the vortex lattice with the periodic pinning structure in thickness-modulated films. In some particular cases the exact equilibrium configurations of the flux-line lattice can be determined in a simple way from a general expression for the free energy of the mixed state. Lowest energy configurations corresponding to resonant coupling with the pinning potential are found when the lattice matches the periodic film structure. We estimate the critical currents to be expected for these situations. In Sec. II, we also consider deviations from a matching configuration. This is an important aspect of experiments dealing with periodic pinning structures, since detailed information concerning the elastic properties of the flux-line lattice can be extracted from the shape of a matching peak in the $j_c(H)$ curves.

In Sec. III, we discuss the dynamic aspects of the interaction in the flux-flow regime of thickness-modulated films. Our phenomenological equation of motion is similar to that considered by Schmid and Hauger¹⁰ for the case of random pinning. Larkin and Ovchinnikov¹⁵ have recently derived this type of equation from the microscopic theory. We restrict our attention to the high-velocity limit where the periodic pinning potential can be treated as a perturbation. We derive results to second order in the perturbing potential for vortex motion under various conditions (with and without electromagnetic radiation, for matching or nonmatching configurations). In particular, the electrodynamic properties of thickness-modulated films are related to the restoring forces arising between the vortices as one deviates from a matching configuration.

II. STATIC INTERACTION

A. General considerations

We consider a superconducting film of variable thickness in a transverse magnetic field $H \approx B$. The film is assumed to be very thin so that its thickness d is everywhere much less than the penetration depth $\lambda(T)$ [$d \ll \lambda(T)$]. If this condition is satisfied, we can neglect additional complications arising from bending of the flux lines.

In order to determine the free energy of the vortex lattice in the pinning potential induced by the thickness variations, we need appropriate expressions for the self-energy of a vortex line as well as for the interaction energy between two flux lines. In the London approach considered here, these quantities can, in principle, be deduced from the magnetic field and supercurrent distributions around a single vortex line obtained by solving London's equation within the superconducting film and Maxwell's equations in free space. For films of variable thickness this is, in general, a rather complicated problem. It is possible, however, to achieve a considerable simplification if one assumes that the vortices are well localized with respect to the variable film profile. By this, we mean that the typical size of a vortex, approximately given by the range $\Lambda = 2\lambda^2/d$ of its electromagnetic screening region in thin films,¹⁶ is much less than the characteristic scale of the thickness variations. For the particular case of films with periodically modulated thickness the local limit considered here corresponds to the condition $\Lambda \ll \lambda_g$, where λ_g is the wavelength of the modulation. We note that because of the long-range repulsive interaction between vortices in thin films¹⁶ the cooperative behavior of the flux lines interacting with the pinning structure is not seriously affected by the local approximation.

In the local limit, the current-field distribution around a flux line can be deduced from that of a vortex in a flat film whose thickness corresponds to that at the vortex position in the layer with spatially varying thickness. The properties of vortices in flat superconducting films have been discussed by Pearl¹⁸ in the limit $d \ll \lambda(T)$ and we shall therefore develop our model using a local formulation of Pearl's work. Whenever possible, however, we shall indicate how results deduced in the local limit should be modified in order to take into account nonlocal effects.

We choose a (two-dimensional) vortex lattice frame of reference as coordinate system. Then, in the local approximation discussed above the self-energy U_i of a vortex line at the lattice site \vec{r}_i can be written as¹⁶

$$U_i = d(\vec{r}_i) \left(\frac{\varphi_0}{4\pi\lambda} \right)^2 \left(\ln \frac{2\Lambda(\vec{r}_i)}{\xi} - \gamma \right) + d(\vec{r}_i) \epsilon_c, \quad (1)$$

where $\Lambda(\vec{r}_i) = 2\lambda^2/d(\vec{r}_i)$ is an effective local penetration depth and ϵ_c is the core condensation energy (per unit length of flux line). For large κ values we can neglect the thickness dependence of ϵ_c .¹⁷ γ is the Euler constant. In a similar way, a simple local generalization of Pearl's results¹⁶ to films with variable thickness leads to the following expression for the interaction energy $W_{i'}$ of two vor-

tices at \vec{r}_i and $\vec{r}_{i'}$:

$$W_{i'} = (\pi/2)(\varphi_0/4\pi\lambda)^2 \{ d(\vec{r}_i) F_0[r_{i'}/\Lambda(\vec{r}_i)] + d(\vec{r}_{i'}) F_0[r_{i'}/\Lambda(\vec{r}_{i'})] \}, \quad (2)$$

where $F_0(z) = H_0(z) - Y_0(z)$ and $r_{i'} = |\vec{r}_i - \vec{r}_{i'}|$. H_0 and Y_0 are, respectively, a Struve and a Neumann function of zero order.

We now apply these general results to the particular case of superconducting films whose thickness is harmonically modulated in one dimension. In the lattice frame of reference introduced above the film profile is described by the following expression:

$$d(\vec{r}) = d + \Delta d \cos \vec{q} \cdot (\vec{r} - \vec{r}_0), \quad (3)$$

where \vec{q} is the wave vector of the modulation ($|\vec{q}| = 2\pi/\lambda_g$) and Δd its amplitude. \vec{r}_0 defines the relative position of the vortex lattice with respect to the thickness modulation. Assuming Δd much smaller than the average film thickness d ($\Delta d/d \ll 1$), one can expand Eqs. (1) and (2) to first order in Δd obtaining the following results for U_i and $W_{i'}$:

$$U_i = \epsilon d + \frac{\Delta d}{2} \left(\epsilon - \frac{\partial \epsilon}{\partial \Lambda} \Lambda \right) \sum_{\vec{q}} e^{i\vec{q} \cdot (\vec{r}_i - \vec{r}_0)}, \quad (4)$$

$$W_{i'} = w_{i'} d + \frac{\Delta d}{4} \left(w_{i'} - \frac{\partial w_{i'}}{\partial \Lambda} \Lambda \right) \times \sum_{\vec{q}} (1 + e^{-i\vec{q} \cdot \vec{r}_{i'}}) e^{i\vec{q} \cdot (\vec{r}_i - \vec{r}_0)}, \quad (5)$$

where $\epsilon = (\varphi_0/4\pi\lambda)^2 [\ln(2\Lambda/\xi) - \gamma] + \epsilon_c$ and $w_{i'} = \pi(\varphi_0/4\pi\lambda)^2 F_0(r_{i'}/\Lambda)$ are the self-energy and interaction energy per unit length of vortex, respectively. In Eqs. (4) and (5), and in the subsequent equations of this paper, the sum is over \vec{q} and $-\vec{q}$ (two terms) and $\vec{r}_{i'} = \vec{r}_i - \vec{r}_{i'}$. It is readily seen that U_i and $W_{i'}$ consist of the usual isotropic terms for the flat-film case and of additional generally anisotropic contributions (proportional to Δd) arising from the thickness modulation.

Having determined U_i and $W_{i'}$ the calculation of the free energy density f is straightforward.¹⁴ We obtain, using Eqs. (4) and (5),

$$f = f_0 + \frac{1}{2A} \sum_{\vec{q}} \left(\Delta \epsilon \sum_i e^{i\vec{q} \cdot (\vec{r}_i - \vec{r}_0)} + \frac{1}{4} \sum_{i'} \Delta w_{i'} (1 + e^{-i\vec{q} \cdot \vec{r}_{i'}}) \times e^{i\vec{q} \cdot (\vec{r}_i - \vec{r}_0)} \right), \quad (6)$$

where $f_0 = n\epsilon + (1/2A) \sum_{i'} w_{i'}$ is the free energy density for a film without thickness modulation, $n = B/\varphi_0$ is the flux-line density, A the specimen area, and the primed sum is over l and l' sepa-

rately omitting the terms $l=l'$. For simplicity we have introduced the quantities

$$\Delta\epsilon = \frac{\Delta d}{d} \left(\epsilon - \frac{\partial\epsilon}{\partial\Lambda} \Lambda \right), \quad (7)$$

and

$$\Delta w_{l'l} = \frac{\Delta d}{d} \left(w_{l'l} - \frac{\partial w_{l'l}}{\partial\Lambda} \Lambda \right). \quad (8)$$

The equilibrium vortex configurations are found by minimizing f with respect to the vortex positions \vec{r}_l . For each flux line l , this gives the condition

$$\nabla_l f_l = 0, \quad (9)$$

where f_l is the free energy per vortex. f and f_l are therefore related by $f = (1/A) \sum_l f_l$. Equation (9) simply states that the total force acting on the vortex l vanishes. These preliminary results can be now used to discuss different situations.

B. Matching configurations

In Ref. 5, we have shown that the vortex lattice matches the periodic film structure when the condition

$$\vec{q} = \vec{g} \quad (10)$$

is satisfied. In Eq. (10), \vec{g} is a vector of the reciprocal vortex lattice. As we shall see in detail below, when Eq. (10) is satisfied the restoring forces between the vortices induced by the pinning potential vanish and one is dealing with an undistorted regular lattice structure. Moreover, by combining Eq. (10) with Eq. (5) one immediately recognizes that the interaction energy $W_{l'l}$ becomes isotropic since $\exp(i\vec{g} \cdot \vec{r}_l) = \exp(i\vec{g} \cdot \vec{r}_{l'}) = 1$ for a periodic structure. Accordingly, we conjecture that, as in flat films,¹⁸ the triangular lattice structure represents the stable configuration in modulated layers at a matching field. In our opinion, however, this is true only in the local limit considered here. In fact, as one can easily imagine, nonlocal effects favor anisotropic current-field distributions around the vortices.¹³ As a consequence, deviations from the triangular structure are expected when Λ becomes comparable with λ_g .

For a triangular lattice, a simple calculation based on the relation $B = (2/\sqrt{3})(\phi_0/a^2)$, where a is the lattice constant, shows that in our local approximation the matching fields $B_{n_1 n_2}$ corresponding to Eq. (10) are given by

$$B_{n_1 n_2} = (\sqrt{3}/2)(\phi_0/\lambda_g^2)(n_1^2 + n_1 n_2 + n_2^2)^{-1}, \quad (11)$$

where n_1 and n_2 are integers. The "fundamental" matching configurations corresponding to $\vec{q} = \vec{g}_1$ (or B_{10}) and $\vec{q} = \vec{g}_2$ (or B_{11}) are shown in Fig. 1. Here, \vec{g}_1 and \vec{g}_2 are first- and second-nearest-

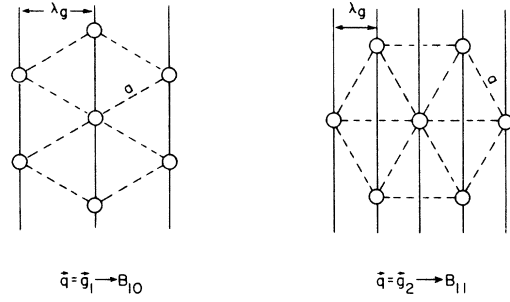


FIG. 1. Fundamental matching configurations $\vec{q} = \vec{g}_1$ and $\vec{q} = \vec{g}_2$ of a triangular vortex lattice in a one-dimensional harmonic pinning structure (represented by the periodic vertical lines). B_{10} and B_{11} are the corresponding matching fields given by Eq. (11).

neighbor vectors of the reciprocal lattice.

Using Eq. (10) the free energy density f given by Eq. (6) can be written as

$$f = f_0 + (n_M \Delta\epsilon + \frac{1}{2A} \sum_{l'l} \Delta w_{l'l}) \cos q r_0, \quad (12)$$

where n_M is the flux-line density corresponding to a matching configuration. In Eq. (12) we have written $\vec{q} \cdot \vec{r}_0 = q r_0$ since \vec{r}_0 can be chosen parallel to \vec{q} without loss of generality. Furthermore, we note that for matching configurations the free energy changes introduced by the thickness modulation are proportional to Δd . In order to evaluate the lattice sum appearing in Eq. (12), we make use of the continuum approximation proposed by Fetter and Hohenberg.¹⁸ In this approach lattice sums are replaced by appropriate integrals over a smooth flux-line density. For our model a simple calculation leads to the following important result

$$\sum_{l'l} \Delta w_{l'l} = 0. \quad (13)$$

Therefore, the interaction energy contribution to the free energy due to the thickness modulation vanishes in the local thin-film limit. It follows that for a matching configuration the important energy variations which couple the vortex lattice with the periodic pinning structure arise only from the vortex self-energy. This clearly results from the expression of f which assumes the simple form

$$f = f_0 + n_M \Delta\epsilon \cos q r_0. \quad (14)$$

The equilibrium position of the lattice with respect to the modulation is found by setting $\partial f / \partial r_0 = 0$. One obtains the condition

$$r_0 = m(\lambda_g/2), \quad (15)$$

where m is an integer. We note that when Eqs. (10) and (15) are simultaneously satisfied the equi-

ilibrium condition Eq. (9) is also satisfied. Moreover, Eq. (15) indicates that both the thickness minima and maxima represent equilibrium positions for the vortices. By considering $\partial^2 f / \partial r_0^2$, however, it is easily seen that when $\Delta\epsilon > 0$ the thickness minima are *stable* equilibrium positions (or pinning lines), whereas for $\Delta\epsilon < 0$ the thickness maxima play the same role. In both cases, the free energy density is $f = f_0 - n_M |\Delta\epsilon|$ and is therefore lower than that of flat films by an amount corresponding to the pinning energy arising from the thickness modulation.

In Eq. (7) both terms, ϵ and $(\partial\epsilon/\partial\Lambda)\Lambda$, contributing to $\Delta\epsilon$ are positive but exhibit different temperature dependences. For the present local model, valid when $\kappa \gg 1$ and $d \ll \lambda(T)$, ϵ is the dominating term at all temperatures, and therefore $\Delta\epsilon > 0$. It is not excluded, however, that for models consistent with a less restrictive choice of κ one can define an "inversion temperature" T^* for which $\Delta\epsilon = 0$, and where the pinning effect switches from the thickness minima ($T > T^*$) to the thickness maxima ($T < T^*$). For $T = T^*$, of course, there is no coupling between the vortex lattice and the periodic pinning structure.

C. Critical currents of matching configurations

Using Eq. (14) it is now possible to calculate the critical current density j_{cM} for a matching configuration. Assuming a uniform transport current flowing parallel to the grooves of the grating-like film surface, j_{cM} is determined by requiring that the Lorentz driving force (per unit volume) $j_{cM} B/c$ equals the maximum value of $|\partial f / \partial r_0|$. This is realized when

$$r_0 = (2m + 1)(\lambda_g/4). \quad (16)$$

Equation (16) shows that the critical state of a matching configuration corresponds to vortices located halfway between the minima and the maxima of the thickness modulation. The critical current density is given by the following expression:

$$j_{cM} = (c/\varphi_0)q |\Delta\epsilon|. \quad (17)$$

Obviously, since at a matching field the vortex lattice assumes its lowest-energy configuration,

the critical currents given by Eq. (17) correspond to (relative) maxima of the $j_c(H)$ curves. Note that j_{cM} is proportional to Δd . Moreover, within the framework of the present model j_{cM} does not depend on the interaction energy between the flux lines and is therefore independent of the matching configuration under consideration. In connection with the possible existence of the inversion temperature T^* defined above, we note that in this case the j_{cM} vs T curve does not exhibit a monotonic behavior but shows a characteristic minimum at $T = T^*$, where j_{cM} vanishes. This unusual temperature dependence of the critical current has been observed in our experiments on thickness-modulated layers.

If one assumes that the contribution to the pinning energy arising from the repulsive interaction between the vortices vanishes also under nonlocal conditions, it is possible to extend the result just derived for j_{cM} to nonlocal situations. According to a general definition of the pinning potential given in Ref. 10 and already used for thickness-modulated films in Ref. 6, one has to replace $\Delta\epsilon$ in Eq. (17) with the following expression:

$$\Delta\Phi(q) = \frac{\Delta d}{d} \left(\Phi(q) - \frac{\partial\Phi(q)}{\partial\Lambda} \Lambda \right), \quad (18)$$

where $\Phi(q)$ is the Hankel transform of the free energy density distribution within a vortex line. Equation (18) reduces to the local expression Eq. (7) for $q = 0$ since by definition $\Phi(0) = \epsilon$. $\Phi(q)$ has been recently calculated by Clem¹⁷ for arbitrary film thicknesses using a vortex model more refined than the one considered here.

D. Deformed vortex lattice—Harmonic approximation

When the matching condition Eq. (10) is not satisfied, one is dealing with a distorted vortex lattice whose equilibrium configuration is determined by the balance of the pinning forces induced by the thickness modulation against the restoring forces between the vortices arising from their mutual electromagnetic repulsive interaction. This clearly results from the equilibrium condition Eq. (9) which can be explicitly written as

$$\frac{i}{2} \Delta\epsilon \sum_{\bar{q}} \bar{q} e^{i\bar{q} \cdot (\bar{r}_l - \bar{r}_0)} + \frac{1}{4} \sum_{\bar{q}} e^{i\bar{q} \cdot (\bar{r}_l - \bar{r}_0)} \sum_{l'} \left(i\bar{q} \Delta w_{ll'} + \frac{\partial \Delta w_{ll'}}{\partial r_{ll'}} (1 + e^{-i\bar{q} \cdot \bar{r}_{ll'}}) \frac{\bar{r}_{ll'}}{r_{ll'}} \right) + \sum_{l'} \frac{\partial w_{ll'}}{\partial r_{ll'}} \frac{\bar{r}_{ll'}}{r_{ll'}} = 0. \quad (19)$$

The first and the second term of this expression are the pinning forces on the vortex l arising from the spatial oscillations of the self-energy and interaction energy, respectively. The third term rep-

resents the response of the vortex lattice to the harmonic pinning force. In the following considerations we shall restrict our attention to a slightly distorted triangular lattice where the vortex posi-

tions are defined by

$$\vec{r}_i = \vec{r}_i^0 + \vec{u}_i, \quad (20)$$

In Eq. (20), \vec{r}_i^0 is a lattice vector of the undistorted triangular lattice and \vec{u}_i represents the displacement of a vortex from its nominal site l . For the subsequent considerations we assume that u_i is much smaller than the period of the thickness modulation ($u_i \ll \lambda_g$). Then, writing the displacement field \vec{u}_i in the form (harmonic approximation)

$$\vec{u}_i = i \sum_{\vec{q}} \vec{u}(\vec{q}) e^{i\vec{q} \cdot (\vec{r}_i^0 - \vec{r}_0^0)}, \quad (21)$$

where the amplitudes $\vec{u}(\vec{q})$ are expected to be proportional to Δd and by expanding the equilibrium condition Eq. (19) to first order in Δd one obtains, using Eq. (13),

$$\frac{1}{2} \Delta \epsilon \vec{q} - \frac{1}{4} \sum_L \frac{\partial \Delta w_L^0}{\partial r_L^0} \frac{\vec{r}_L^0}{r_L^0} \sin(\vec{q} \cdot \vec{r}_L^0) + \underline{D}(\vec{q}) \vec{u}(\vec{q}) = 0, \quad (22)$$

where $\Delta w_L^0 = \Delta w(r_L^0)$ and $\underline{D}(\vec{q})$ is the ‘‘dynamical matrix.’’ In Eq. (22) we have introduced a single index L for the lattice sum since we have taken the lattice point l as the origin of coordinates in the sums over l' appearing in Eq. (19). Using the notation of Fetter and Hohenberg,¹⁸ the dynamical matrix $\underline{D}(\vec{q})$ can be written as

$$\underline{D}(\vec{q}) = \frac{4\pi}{\bar{\kappa}} \left(\frac{\varphi_0}{4\pi\lambda} \right)^2 \begin{pmatrix} [\eta(\vec{q}) - \xi(\vec{q})] & \alpha(\vec{q}) \\ \alpha(\vec{q}) & [\eta(\vec{q}) + \xi(\vec{q})] \end{pmatrix}, \quad (23)$$

where $\bar{\kappa}$ is the circulation about a vortex. $\eta(\vec{q})$, $\xi(\vec{q})$, and $\alpha(\vec{q})$ denote lattice sums involving the interaction energy and its derivatives. To solve Eq. (22) for $\vec{u}(\vec{q})$, it is convenient to introduce normal coordinates¹⁰ which diagonalize the dynamical matrix in Eq. (23). In this particular representation, $\vec{u}(\vec{q})$ is given by

$$\vec{u}(\vec{q}) = -\frac{1}{2} \sum_p \vec{e}_p \left[(\vec{q} \cdot \vec{e}_p) \Delta \epsilon - \frac{1}{2} \sum_L \frac{\partial \Delta w_L^0}{\partial r_L^0} \left(\frac{\vec{r}_L^0}{r_L^0} \cdot \vec{e}_p \right) \times \sin(\vec{q} \cdot \vec{r}_L^0) \right] / D_p(\vec{q}), \quad (24)$$

where \vec{e}_p is a unit vector describing longitudinal ($p=l$) or transverse ($p=t$) polarizations. For deformations propagating along symmetry directions of the triangular lattice the \vec{e}_p 's are defined by the following relations

$$\vec{e}_l \cdot \vec{k} = k, \quad \vec{e}_t \cdot \vec{k} = 0, \quad (25)$$

where \vec{k} is the wave vector of the deformation confined to the first Brillouin zone. Hence, \vec{q} and \vec{k} are related by

$$\vec{q} = \vec{k} + \vec{g}. \quad (26)$$

The force constants $D_p(\vec{q})$'s are periodic functions in the reciprocal lattice,^{10,18} i.e., $D_p(\vec{q} + \vec{g}) = D_p(\vec{q}) = D_p(\vec{k})$. They are related to the lattice sums $\eta(\vec{k})$, $\xi(\vec{k})$ and $\alpha(\vec{k})$ by the following relation:

$$D_p(\vec{k}) / \mu = \eta(\vec{k}) \pm [\xi^2(\vec{k}) + \alpha^2(\vec{k})]^{1/2}, \quad (27)$$

where the plus and minus sign correspond to $p=l$ and $p=t$, respectively. μ is the factor multiplying the matrix in Eq. (23). An important consequence of the long-range repulsive interaction between vortices in very thin films is that the lattice is essentially incompressible ($D_l \gg D_t$) for long-wavelength deformations ($ka \ll 1$).^{10,19-21} As a consequence, longitudinal deformations may be neglected in this limit. We don't know if this is still valid for short wavelengths. Since such deformations are important in a vortex lattice interacting with a harmonic pinning structure, we shall consider both the l and t components in Eq. (24).

Since the D_p 's vanish for $\vec{k}=0$, from their periodicity it follows that $D_p(\vec{g})=0$. Therefore, for matching configurations the lattice restoring forces induced by the periodic pinning structure vanish. As a consequence, the harmonic approximation considered here leads to divergent deformation amplitudes [Eq. (24)] for $\vec{q}=\vec{g}$. In some respects, this result shows that matching configurations correspond to ‘‘resonant’’ coupling¹³ of the vortex lattice with the periodic pinning structure. On the other hand, however, this also shows the limits of the harmonic approximation which applies only as long as $u(\vec{q}) \ll \lambda_g$. This condition calls for pinning forces much smaller than the restoring forces $D_p(\vec{k})\lambda_g$ corresponding to vortex displacements of the order of λ_g (weak pinning limit). When B is sufficiently close to a matching field, however, the weak-pinning condition is no longer satisfied since, independently of the strength of the pinning forces, $D_p(\vec{k}) \rightarrow 0$ as $\vec{q} \rightarrow \vec{g}$. In this case, other models should be considered in order to describe the exact nature of the transition to a matching configuration.

Having determined \vec{u}_i to first order in Δd , we can now calculate the free energy density in the harmonic approximation by expanding Eq. (6) to second order in Δd . The calculations are simple but rather long so that we shall not give the details here. The resulting expression for f assumes the simple form

$$f = f_0 + n\Delta\epsilon \{ \delta_{\vec{q}, \vec{g}} \cos q r_0 + [\vec{u}(\vec{q}) \cdot \vec{q}] (1 - \delta_{2\vec{q}, \vec{g}} \cos 2q r_0) \} \\ - \frac{1}{2} n \sum_L' \frac{\partial \Delta w_L^0}{\partial r_L^0} \left(\frac{\vec{r}_L^0}{r_L^0} \cdot \vec{u}(\vec{q}) \right) \sin(\vec{q} \cdot \vec{r}_L^0) + n \sum_p D_p(\vec{k}) u_p^2(\vec{q}) (1 - \delta_{2\vec{q}, \vec{g}} \cos 2q r_0), \quad (28)$$

where the $u_p(\vec{q})$'s are the l and t components of $\vec{u}(\vec{q})$ in Eq. (24) and $\delta_{\vec{q}, \vec{g}}$ is the Kronecker δ . In deriving Eq. (28) we have used the inversion symmetry of the triangular lattice and Eq. (13) in order to eliminate several terms involving complicated lattice sums. In Eq. (28), energy contributions involving $\Delta\epsilon$ and Δw_L^0 arise from the harmonic pinning structure, whereas those proportional to $D_p(\vec{k})$ are related to the elastic deformation energy stored in the distorted lattice.

For $\vec{q} = \vec{g}$, a condition automatically implying that $2\vec{q}$ is also a reciprocal lattice vector, the terms of f containing $\vec{u}(\vec{q})$ diverge as shown in our previous discussion. This indicates that the above expression for f is no longer valid in the particular case of matching configurations. Note, however, that in Eq. (28) the contributions to f independent of $\vec{u}(\vec{q})$ give exactly the free energy density found previously for the matching case [Eq. (14)].

Several interesting situations can be now discussed with the aid of Eq. (28).

E. Bragg configurations ($2\vec{q} = \vec{g}$)

An interesting situation arises when the vortex lattice does *not* match the harmonic pinning structure but satisfies the condition $2\vec{q} = \vec{g}$. In this case, the representative point associated with the wave vector \vec{k} of the harmonic lattice deformation lies exactly on the Brillouin zone boundary. For this reason we call "Bragg configurations" vortex configurations defined by the relation $2\vec{q} = \vec{g}$. It must be noted, however, that the $2\vec{q} = \vec{g}$ configurations considered in this paper are not the only ones satisfying the Bragg condition. Their distinctive property is that \vec{k} is parallel to a high-symmetry direction of the triangular lattice ($\vec{k} = \frac{1}{2}\vec{g}_1$) and therefore Eq. (25) applies. As an example, in Fig. 2 we illustrate in reciprocal space the particular case $2\vec{q} = \vec{g}_4$, where \vec{g}_4 is a fourth-nearest-neighbor vector of the reciprocal lattice. The magnetic field B corresponding to the situation shown in Fig. 2 is such that $B_{11} < B < B_{10}$ [$B = (2\sqrt{3}/7)\varphi_0/\lambda_g^2$].

The vector relation $2\vec{q} = \vec{g}$ not only implies well-defined values, $B = 4B_{n_1 n_2}$, of the magnetic field but also well-defined orientations of the vortex lattice with respect to the thickness modulation. Accordingly, one could wonder whether Bragg configurations are or are not equilibrium configurations of the vortex lattice. For $B = 4B_{n_1 n_2}$, in

fact, the vortex lattice could assume its equilibrium configurations by selecting orientations different from those predicted by $2\vec{q} = \vec{g}$. A definitive conclusion concerning this point requires, of course, a complete study of the free energy density given by Eq. (28). This, in turn, implies a detailed knowledge of the \vec{k} dependence of the force constants. Unfortunately, this information is not available so far. Nevertheless, preliminary considerations indicate that some Bragg configurations are actually equilibrium configurations of the vortex lattice, whereas others are not. For instance, the configuration $2\vec{q} = \vec{g}_4$ of Fig. 2 is believed to be an equilibrium lattice configuration for the following reasons. As B varies from B_{11} to B_{10} , \vec{q} describes in reciprocal space a certain path connecting the fundamental matching configurations $\vec{q} = \vec{g}_2$ and $\vec{q} = \vec{g}_1$. As a consequence, for some value of B lying between B_{11} and B_{10} the corresponding \vec{k} vector must reach the Brillouin zone boundary. It will be subsequently shown that the energy gain of the vortex lattice due to the pinning structure is inversely proportional to the $D_p(\vec{k})$'s which on the zone boundary are expected to assume their minimum value for $\vec{k} = \frac{1}{2}\vec{g}_1$. Hence, among the lattice configurations showing deformations characterized by \vec{k} vectors reaching the Brillouin zone boundary those satisfying the condition $2\vec{q} = \vec{g}$ are believed to have the lowest energy. For $B_{11} < B < B_{10}$ there are two possible Bragg configurations, namely those

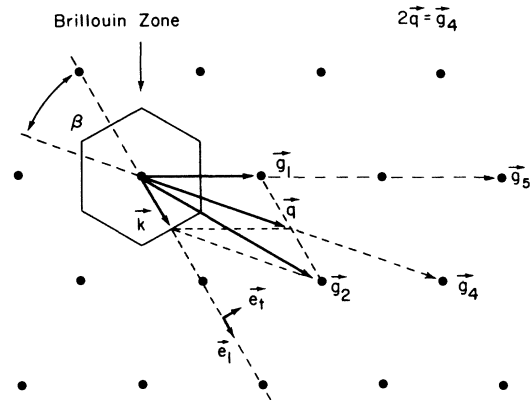


FIG. 2. Geometrical relationship (in reciprocal space) between wave vector \vec{q} of the thickness modulation and wave vector \vec{k} of the pinning-induced deformation for the Bragg configuration $2\vec{q} = \vec{g}_4$. The polarization vectors \vec{e}_1 and \vec{e}_2 are also shown.

defined by $2\vec{q} = \vec{g}_4$ and $2\vec{q} = \vec{g}_5$ (Fig. 2). The last one, however, is unlikely an equilibrium lattice configuration, the corresponding magnetic field $B = (4/3)B_{11}$ being too close to B_{11} . For this field, in fact, \vec{q} is more conveniently located near \vec{g}_2 , where smaller \vec{k} vectors favor configurations of lower energy (Sec. II F). One is left with the possibility $2\vec{q} = \vec{g}_4$ which in our opinion represents an equilibrium configuration of the vortex lattice.

The free energy density of a Bragg configuration can be written as

$$f = f_0 - n \sum_{\vec{p}} D_p(\vec{k}) u_p^2(\vec{q})(1 - \cos 2qr_0), \quad (29)$$

where $\vec{u}_p(\vec{q})$ is given by

$$\vec{u}_p(\vec{q}) = -\frac{1}{2}(\vec{q} \cdot \vec{e}_p) [\Delta\epsilon / D_p(\vec{k})] \vec{e}_p. \quad (30)$$

These simple expressions have been deduced from Eqs. (24) and (28) by noting that the lattice sum appearing in these equations vanishes for $2\vec{q} = \vec{g}$. Note that the free energy change $\Delta f = f_0 - f$ is proportional to $(\Delta d)^2$, whereas for matching configurations we found $\Delta f \propto \Delta d$. Moreover, for some Bragg configurations the polarization factor $\vec{q} \cdot \vec{e}_i$ (or $\vec{q} \cdot \vec{e}_i$) appearing in Eq. (30) vanishes. This happens, for instance, when $2\vec{q} = \vec{g}_2$ ($\vec{q} \cdot \vec{e}_1 = 0$) or $2\vec{q} = \vec{g}_1$ ($\vec{q} \cdot \vec{e}_2 = 0$). For such configurations no coupling exists between the harmonic pinning structure and the longitudinal (or transverse) deformations of the vortex lattice.

The position of the vortex lattice with respect to thickness modulation is determined by the conditions $\partial f / \partial r_0 = 0$ and $\partial^2 f / \partial r_0^2 > 0$. This leads to

$$r_0 = (2m + 1)(\lambda_g / 4). \quad (31)$$

Bragg configurations obeying Eq. (31) are shown in Fig. 3, where for clarity we first illustrate the case $2\vec{q} = \vec{g}_1$ by means of a one-dimensional vortex chain [Fig. 3(a)]. Then, in Fig. 3(b) we show a two-dimensional picture of the deformed triangular lattice corresponding to the condition $2\vec{q} = \vec{g}_4$ illustrated in Fig. 2. In deducing this lattice configuration, we have considered only transverse deformations and have made use of the property that for a triangular structure the lattice in real space is rotated by 30° with respect to the corresponding one in reciprocal space. Moreover, the wavelength $2\pi/k$ of the shear deformation shown in Fig. 3(b) turns out to be $\sqrt{7}\lambda_g$ and its direction of propagation (parallel to \vec{k}) makes an angle β , satisfying the relation $\sin\beta = \sqrt{3}/7$, with the wave vector \vec{q} of the thickness modulation. These numerical results are easily deduced from Fig. 2. Note that Fig. 3 clearly shows the pinning effect of the thickness minima acting as attractive trap chains for the flux lines.

From Eqs. (29)–(31) it follows that the free energy density of a *stable* Bragg configuration is

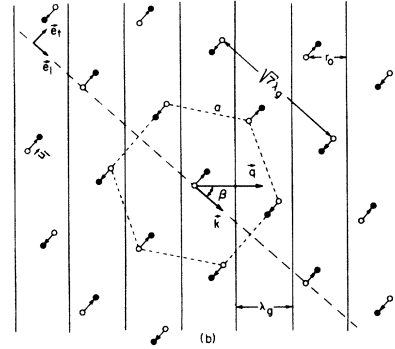
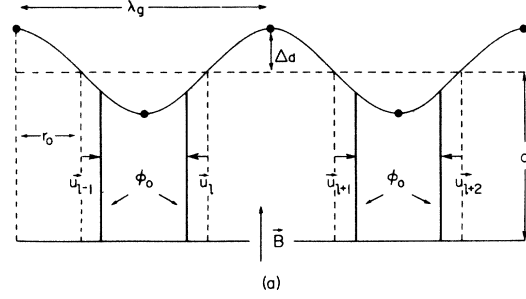


FIG. 3. (a) Bragg configuration $2\vec{q} = \vec{g}_1$ of a one-dimensional vortex chain in a thickness-modulated film. Also shown is the longitudinal deformation of the chain. Dots at the thickness maxima and minima indicate vortex positions for the undistorted but not stable $2\vec{q} = \vec{g}_1$ configuration. (b) Vortex lattice configuration satisfying the $2\vec{q} = \vec{g}_4$ Bragg condition illustrated in Fig. 2. The corresponding magnetic field is $B = (2\sqrt{3}/7)(\phi_0/\lambda_g^2)$. The periodic vertical lines represent maxima of the thickness modulation. Open circles denote vortex positions in the undistorted triangular lattice. The pinning-induced (transverse) deformation propagates in the \vec{k} direction and has wavelength $\sqrt{7}\lambda_g$. Note the attractive effect of the thickness minima (pinning lines). $r_0 = (3/4)\lambda_g$ is given by Eq. (31).

given by

$$f = f_0 - \frac{1}{2}n(\Delta\epsilon)^2 \sum_{\vec{p}} \frac{(\vec{q} \cdot \vec{e}_p)^2}{D_p(\vec{k})}. \quad (32)$$

In this connection, we note that the equilibrium condition $\partial f / \partial r_0 = 0$ also predicts the existence of regular ($\vec{u}_i = 0$ at all lattice sites i) but *unstable* ($\partial^2 f / \partial r_0^2 < 0$) lattice structures when $r_0 = n(\lambda_g/2)$. As shown in Fig. 3(a), such configurations correspond to vortex lines located alternately at the maxima and minima of the thickness modulation. Their energy $f = f_0$, however, is larger than that of the distorted but stable configurations considered above [Eq. (32)]. Hence, we conclude that the harmonic pinning potential favors the formation of a distorted vortex-lattice structure.

In a Bragg configuration the vortex lattice interacts with the pinning structure of thickness-modulated films by means of short-wavelength defor-

mations ($ka \sim 1$). This appears to be a distinctive feature of harmonic pinning structures. In random pinning structures, in fact, the lattice usually responds to weak pinning forces as an elastic continuum ($ka \ll 1$).^{10,20,21} The important point here is that a vortex lattice interacting with a random pinning structure can generally reach its equilibrium configuration by selecting only those fluctuations of the pinning potential whose wavelengths are comparable with a . Over a relatively wide range of flux-line densities one is therefore dealing with a selective "quasi-matching" effect which automatically leads to long-wavelength deformations. In the case of a harmonic pinning structure, on the other hand, such long-wavelength deformations are clearly impossible for large deviations from a matching configuration (as is precisely the case for a Bragg configuration) since a single Fourier component plays the dominant role in the pinning potential and consequently no alternative choice is left to the vortex lattice in finding its equilibrium configuration.

Using the method of Sec. II C, one can very easily determine the critical current density j_{cB} for Bragg configurations. From Eqs. (29) and (30) one obtains

$$j_{cB} = (c/\varphi_0) q (\Delta\epsilon)^2 \sum_p \frac{(\vec{q} \cdot \vec{e}_p)^2}{2D_p(\vec{k})}. \quad (33)$$

The critical state corresponds to $r_0 = (2m+1)(\lambda_g/8)$. Equation (31) shows that j_{cB} is proportional to $(\Delta d)^2$ and depends on the Bragg configuration under consideration through the characteristic angle β [Figs. 2 and 3(b)] appearing in the polarization factor $\vec{q} \cdot \vec{e}_p$. Since the force constants D_p 's are functions of the flux-line density, j_{cB} also depends on the magnetic field $B = 4B_{n_1 n_2}$ defining the corresponding Bragg configuration.

A concrete estimate of f and j_{cB} requires the calculation of the force constants $D_p(\vec{k})$'s for $\vec{k} = \frac{1}{2}\vec{g}_1$. In principle, this can be done by performing the lattice sums¹⁸ $\eta(\vec{k})$, $\xi(\vec{k})$, and $\alpha(\vec{k})$ appearing in Eq. (27). As far as $D_1(\vec{k})$ is concerned, to our knowledge a similar calculation has not yet been attempted for the case $ka \sim 1$ considered here. On the contrary, $D_t(\vec{k})$ can be easily estimated by comparing the last term of Eq. (28) corresponding to the deformation energy stored in the vortex lattice with an analogous expression obtained by Conen and Schmid¹⁹ for transverse deformations propagating in the \vec{g}_1 direction. A straightforward calculation leads to

$$D_t(\vec{g}_1/2) = 4.62 C_{66}, \quad (34)$$

where C_{66} is the shear modulus of the vortex lattice.¹⁹⁻²¹ Since $\vec{k} = \frac{1}{2}\vec{g}_1$ reaches the Brillouin zone boundary, Eq. (34) is believed to give the largest

value of the force constant for shear deformations propagating in the \vec{g}_1 direction.

F. Vortex configurations for $ka \ll 1$

By combining Eq. (24) with Eq. (28), the free energy density of vortex configurations which do not satisfy the conditions $\vec{q} = \vec{g}$ or $2\vec{q} = \vec{g}$ turns out to be $f = f_0 - n \sum_p D_p(\vec{k}) u_p^2(\vec{q})$.

In the following we restrict our attention to vortex configurations characterized by long-wavelength deformations of the vortex lattice ($ka \ll 1$). According to Eq. (26), such lattice distortions occur when \vec{q} slightly deviates from a reciprocal lattice vector \vec{g} , i.e., when B is relatively close to a matching field $B_{n_1 n_2}$. In this connection we remember that the harmonic approximation no longer applies when B is too close to $B_{n_1 n_2}$. For this reason the following considerations are valid only under rather restrictive conditions we shall specify later on. Nevertheless, the approach described below is considered very useful since it provides the basis for an interpolation procedure leading to a significant improvement of our model.

In the long-wavelength limit ($ka \ll 1$) transverse deformations of the vortex lattice predominate.^{10, 19-21} The corresponding force constant is given by $D_t(\vec{k}) = K_t k^2$, where $K_t = C_{66} \varphi_0 / B$. D_t is isotropic since the lattice has hexagonal symmetry. For the same reason Eq. (25) is valid for all \vec{k} directions in the limit $ka \ll 1$. Then, using Eq. (24) for $\vec{u}_t(\vec{q})$ and the notation of Fig. 4, the free energy density of vortex configurations close to the matching configuration $\vec{q} = \vec{g}$ can be written as

$$f = f_0 - \frac{1}{4} n [(\Delta\epsilon)^2 / K_t] b \sin^2 \varphi / (1 + b - 2\sqrt{b} \cos \varphi)^2, \quad (35)$$

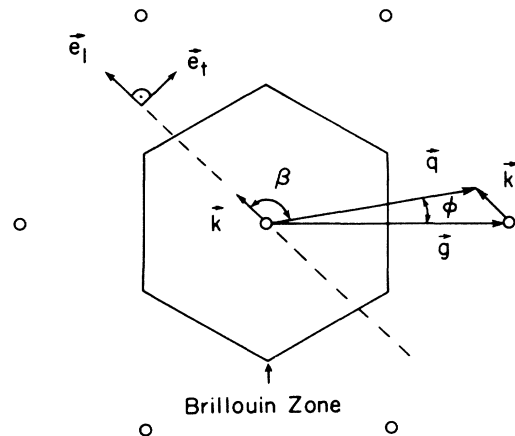


FIG. 4. Geometrical relationship (in reciprocal space) between \vec{g} , \vec{q} , and \vec{k} for small deviations ($ka \ll 1$) from the matching configuration $\vec{q} = \vec{g}$.

where $b = (q/g)^2 = (B_{n_1 n_2}/B)$. In deriving Eq. (35), we have neglected the contribution to $\tilde{u}_i(\tilde{q})$ in Eq. (24) arising from the spatial oscillations of the interaction energy. This term vanishes for $\tilde{q} = \tilde{g}$ and therefore, compared to the self-energy contribution, is expected to be small in the limit $ka \ll 1$. The angle φ defining the orientation of the vortex lattice with respect to the thickness modulation (Fig. 4) is obtained from the equilibrium condition $\partial f/\partial \varphi = 0$. This leads to

$$\cos \varphi = 2\sqrt{b}/(1+b). \quad (36)$$

Note that $\cos \varphi \leq 1$ for all values of b and that, as expected, $\varphi = 0$ for $b = 1$. Using simple trigonometry and Eq. (36), one easily deduces magnitude and direction of the wave vector \tilde{k} characterizing the shear deformation of the vortex lattice. One obtains

$$k^2 = q^2(1-b)^2/b(1+b) \approx \frac{1}{2}q^2(1-b)^2, \quad (|1-b| \ll 1), \quad (37)$$

and

$$\sin^2 \beta = (\tilde{e}_q \cdot \tilde{e}_i)^2 = (1+b)^{-1}, \quad (38)$$

where \tilde{e}_q is a unit vector parallel to the wave vector \tilde{q} of the thickness modulation. Using these results, it is now possible to construct a picture of the deformed vortex lattice (corresponding to a given value of b) with the method already applied to the Bragg configuration of Fig. 3(b). In the present case, however, the coordinate r_0 which together with φ defines the position of the lattice with respect to the thickness modulation is undetermined. As a matter of fact, the free energy density [Eq. (28)] is generally independent of r_0 in the harmonic approximation.

From Eqs. (35) and (36) we deduce the following expression for the equilibrium free energy density:

$$f = f_0 - \frac{1}{4} n_M [(\Delta \epsilon)^2 / K_t] / (1-b)^2. \quad (39)$$

As expected, our model leads to a divergent expression of f for $b = 1$. Actually, Eq. (39) is valid only as long as the harmonic approximation applies, i.e., when $u_i(\tilde{q}) \ll \lambda_g$. This is equivalent to requiring that $\Delta \epsilon \ll K_t(1-b)^2$, a rather stringent condition for the pinning structure since we are already considering situations where $(1-b)^2 \ll 1$. It is possible, however, to extend the present discussion to the matching case ($b = 1$) by performing a simple interpolation of Eq. (14) [where r_0 assumes the equilibrium value given by Eq. (15)] and Eq. (39). This leads to the following expression for the free energy density of vortex configurations such that $|B - B_{n_1 n_2}| \ll B_{n_1 n_2}$:

$$f = f_0 - n_M \Delta \epsilon [1 + (4K_t/\Delta \epsilon)(1-b)^2]^{-1}. \quad (40)$$

This relation has the expected minimum [Eq. (14)] for $b = 1$ and changes precisely into Eq. (39) when $\Delta \epsilon \ll K_t(1-b)^2$. Using Eq. (37), in the opposite limit $\Delta \epsilon \gg K_t(1-b)^2$ Eq. (40) can be written as

$$f = f_0 - n_M \Delta \epsilon + 8C_{66}(k/q)^2. \quad (41)$$

The following model²² provides a physical interpretation of the interpolation leading to Eq. (40). For simplicity, we restrict our attention to the one-dimensional situation shown in Fig. 5, where a single vortex chain interacts with the harmonic pinning potential of a thickness-modulated film. Let us first consider a perfectly rigid vortex chain. Then, a possible configuration corresponding to a nonmatching state is that shown in Fig. 5(a). Obviously, its free energy density is the same as that of the pinning-free vortex chain, i.e., $f = f_0$. In order to simulate the situation occurring in the limit $\Delta \epsilon \gg K_t(1-b)^2$ in which we are interested here, we turn off the interaction among the vortices of the chain. Then, the resulting configuration is that shown in Fig. 5(b), where the vortices are located at the bottom of the potential wells of the harmonic pinning structure.

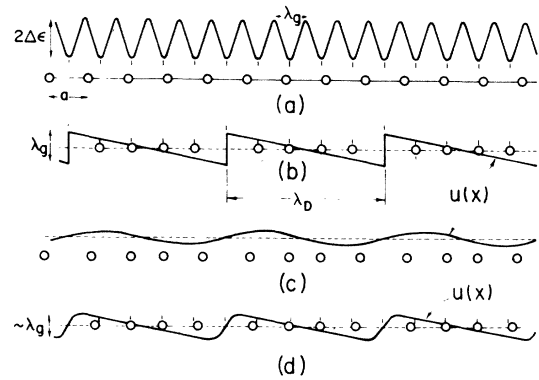


FIG. 5. One-dimensional vortex chain in a harmonic pinning structure. Shown are nonmatching configurations and deformations $u(x)$ of the vortex chain corresponding to different strengths of its force constant $D(k)$. (a) Rigid reference vortex chain [$D(k) = \infty$]. (b) Formation of a vortex-defect superlattice with period $\lambda_D = a\lambda_g / (a - \lambda_g)$ in the case of a soft vortex chain [$D(k) = 0$]. (c) Vortex chain in the harmonic approximation [$D(k)\lambda_g \gg q\Delta\epsilon$]. For clarity the amplitude of $u(x)$ has been slightly exaggerated. (d) Vortex chain in the limit $D(k)\lambda_g \ll q\Delta\epsilon$ showing superlattice structure of (b) locally distorted at the defect sites, where $u(x)$ is smoothed out by the finite vortex-vortex interaction. Note that $D(k)$ is actually controlled by the magnetic field which determines a and, hence, $k = 2\pi/\lambda_D$. For given λ_g and $\Delta\epsilon$ (c) and (d) correspond therefore to different B values. In (d) λ_D should be larger than in (c). (d) represents therefore the chain configuration closer to the matching case ($a = \lambda_g$).

However, since the initial configuration [Fig. 5(a)] was a nonmatching one, an array of vacancies ($a > \lambda_g$) or interstitials ($a < \lambda_g$) develops along the vortex chain. One can easily verify that for commensurate situations $ma = n\lambda_g$ such that $N|n - m| = m$, where N , m , and n are integers, the defect array is periodic. The period $\lambda_D = 2\pi/k$ of the resulting vortex-defect "superlattice" is determined by Eq. (26). For instance, in Fig. 5 the relevant \vec{g} vector is $\vec{g}_1 (g_1 = 2\pi/a)$. Accordingly, from Eq. (26) one deduces $\lambda_D = a\lambda_g/|a - \lambda_g|$. Using a continuum approximation ($\lambda_D \gg a$) in Fig. 5(b) we also show the displacement $u(x)$ of the vortices from their equilibrium positions in the rigid reference chain [Fig. 5(a)]. $u(x)$ is a periodic function of x (period λ_D) showing linear regions between successive chain defects. Discontinuities of magnitude λ_g appear in $u(x)$ at the defect sites. The free energy density of the soft vortex chain of Fig. 5(b) is $f = f_0 - n\Delta\epsilon$.

We now turn on a finite repulsive interaction among the vortices. Then, two drastically different situations can occur. If the force constant $D(k)$ of the chain is such that $q\Delta\epsilon \ll D(k)\lambda_g$, from Sec. IID we know that the resulting deformation of the vortex row is harmonic [Fig. 5(c)]. The situation shown in Fig. 5(c) corresponds, therefore, to the two-dimensional case $\Delta\epsilon \ll K_t(1-b)^2$ discussed in detail above. Note that in the harmonic approximation the superlattice structure is washed out by the repulsive interaction between the vortices. In contrast, in the opposite limit $q\Delta\epsilon \gg D(k)\lambda_g$ corresponding to vortex configurations very close to the matching one ($n \approx n_M$, $\lambda_D \gg \lambda_g$) the superlattice is not seriously affected by the vortex-vortex interaction, whose main effect is to smooth out the discontinuities in $u(x)$ at the defect sites [Fig. 5(d)]. Since the resulting chain distortion does not significantly differ from that of the soft vortex chain of Fig. 5(b), the energy density gain f_p due to the pinning potential will be nearly the same as in that case, i.e., $f_p \approx -n_M\Delta\epsilon$. Because of the finite interaction, however, we have now to take into account the deformation energy stored in the distorted chain. In this connection we note that large portions of the vortex chain shown in Fig. 5(d) behave as an elastic continuum, characterized by $D(k) = Kk^2$, where the strain $\partial u/\partial x$ is small and nearly uniform: $\partial u/\partial x \approx \lambda_g/\lambda_D = k/q$. Accordingly, the elastic energy density associated with these regions is $f_e \approx \frac{1}{2}C(k/q)^2$, where $C = Kn \approx K/\lambda_g$ is the elastic modulus of the chain. There is, of course, additional deformation energy stored in the regions, of size $\sim \lambda_g$, surrounding the defects, where the rapid variation of $u(x)$ precludes the use of elasticity theory. Compared to f_e , however, this contribution is expected to be small. Thus, taking

into account both f_p and f_e , the free energy density of the vortex chain of Fig. 5(d) becomes $f \approx f_0 - n_M\Delta\epsilon + \frac{1}{2}C(k/q)^2$, an expression very similar to that [Eq. (41)] resulting from the interpolation procedure in the corresponding limit $\Delta\epsilon \gg K_t(1-b)^2$. For this reason, although at present very little is known about the structure of the superlattice and its deformation in the two-dimensional case, the interpolation approach discussed above is considered basically correct.

We now focus our attention on the critical currents of thickness-modulated films under nearly matching conditions ($|B - B_{n_1 n_2}| \ll B_{n_1 n_2}$). In this connection, it is useful to briefly reconsider the case of a matching configuration. For $j \leq j_{cM}$ all flux lines of the lattice are simultaneously prevented from moving by an identical energy barrier Δ which varies with current from $\Delta = 2\Delta\epsilon$ for $j = 0$ to $\Delta = 0$ for $j = j_{cM}$. The presence of this uniform energy barrier is reflected in the coupling energy $\Delta\epsilon$ appearing in the expression for j_{cM} [Eq. (17)]. Suppose now that the vortex lattice deviates from a matching configuration. In this case, the vortex lattice responds to the harmonic pinning force by exerting a restoring force on the flux lines. Because of this additional coupling with the whole lattice, the vortices, in contrast with the matching case, no longer interact with the pinning potential and the transport current as independent units. Under these circumstances the exact calculation of j_c amounts to determining the "critical" positions of the vortices from the set of coupled nonlinear equations $\nabla_t f_t = (\vec{j} \times \vec{\phi}_0)/c$ describing their static equilibrium in presence of a finite transport current. Though rather complex, such a calculation would have the merit of specifying the role of a defect in triggering the elastic instability¹⁷ of the vortex-defect superlattice [Fig. 5(d)] as j reaches j_c . In this connection, we emphasize that the formation of lattice defects is essential for the occurrence of a finite critical current. We have seen, in fact, that with the exception of Bragg configurations the volume pinning force $\partial f/\partial r_0$ vanishes for a harmonically distorted lattice [Fig. 5(c)]. For nonmatching situations a significant pinning effect is expected only when a fairly resolved defect array develops in the vortex lattice. According to our previous considerations, this will be the case when $q\Delta\epsilon \gtrsim D(k)\lambda_g$ or, equivalently, when $\Delta\epsilon \gtrsim K_t(1-b)^2$.

In the following, we estimate j_c with an approximate method based on the energy-barrier picture discussed above. It seems reasonable to assume that for nearly matching configurations Eq. (17) still applies provided that $\Delta\epsilon$ is replaced by a lower energy barrier reflecting the effect of lattice rigidity. As one can easily imagine, the

periodic lattice deformation induced by the pinning structure spatially modulates the energy barrier experienced by the vortices. Elementary considerations show that for $j=0$ the space average of $\Delta(\vec{r}_1)$ is $\sim 2\Delta f/n_M$, where $\Delta f=f_0-f$ is given by Eq. (40). Hence, replacing $\Delta f/n_M$ for $\Delta\epsilon$ in Eq. (17) and remembering that $B \approx B_{n_1 n_2}$, one obtains

$$\frac{j_c}{j_{cM}} \approx \frac{\Delta\epsilon}{4K_t} \left[\left(\frac{\Delta\epsilon}{4K_t} \right) + \left(\frac{B}{B_{n_1 n_2}} - 1 \right)^2 \right]^{-1}. \quad (42)$$

Thus, in our approximation a matching peak centered at $B=B_{n_1 n_2}$ has a resonantlike shape. The width of the critical current resonance is controlled by the ratio $\Delta\epsilon/K_t$, where $\Delta\epsilon$ represents the pinning effect and K_t the elastic response of the vortex lattice. As expected, for a given thickness modulation a large stiffness of the lattice ($\Delta\epsilon \ll K_t$) favors the formation of sharp matching peaks, whereas for a soft lattice ($\Delta\epsilon \gg K_t$) the j_c resonances are washed out.

Finally, we briefly discuss the interaction of a rather dense vortex lattice ($a \ll \lambda_g$) with the harmonic pinning structure. In this case, \vec{q} is confined within the first Brillouin zone and therefore $\vec{k}=\vec{q}$. Since Eq. (25) applies when $qa \ll 1$, it follows that $\vec{e}_t \cdot \vec{q} = 0$ and $\vec{e}_t \cdot \vec{q} = q$. Moreover, by transforming the lattice sum appearing in Eq. (24) into an integral over a smooth flux-line density, one can easily verify that the transverse part of this term vanishes. Therefore, from Eq. (24) one deduces $\vec{u}_t(\vec{q})=0$. We conclude that for $qa \ll 1$, i.e., $B \gg B_{10}$, the vortex lattice couples with the harmonic pinning potential only by means of *longitudinal* deformations. If one neglects the small contribution to $\vec{u}_l(\vec{q})$ arising from the longitudinal part of the lattice sum in Eq. (24), the free energy density can be written as

$$f = f_0 - \frac{1}{4} n(q\Delta\epsilon)^2 / D_1(\vec{q}), \quad (43)$$

where²¹ $D_1(\vec{q}) = (B\varphi_0/2\pi d)q$ for very thin films ($d \ll \lambda$) in the limiting case $qa \ll 1$.

$$\nabla_l f_l = \frac{i}{2} \Delta\epsilon \sum_{\vec{q}} \vec{q} e^{i\vec{q} \cdot (\vec{r}_l - \vec{r}_0)} + \frac{1}{4} \sum_{\vec{q}} e^{i\vec{q} \cdot (\vec{r}_l - \vec{r}_0)} \sum_{l'} \left(i \vec{q} \Delta w_{ll'} + \frac{\partial \Delta w_{ll'}}{\partial r_{ll'}} (1 + e^{-i\vec{q} \cdot \vec{r}_{ll'}}) \frac{\vec{r}_{ll'}}{r_{ll'}} \right) + \sum_{l'} \frac{\partial w_{ll'}}{\partial r_{ll'}} \frac{\vec{r}_{ll'}}{r_{ll'}}, \quad (45)$$

an expression containing terms describing the oscillating pinning force and the lattice restoring force (Sec. IID).

We note that Eq. (44) is a phenomenological equation of motion.¹⁰ At large flux-flow velocities (see Sec. IIIC), however, Eq. (44) becomes essentially similar to an analogous equation of motion derived by Larkin and Ovchinnikov¹⁵ from the microscopic theory. The main difference is that these authors describe the effect of pinning by

III. DYNAMIC INTERACTION

A. Equation of motion

When the transport current I flowing parallel to the grooves of the harmonic film profile exceeds the critical value I_C ($I > I_C$), the mixed state enters the flux-flow regime. In order to investigate the dynamic interaction of the whole vortex lattice with the pinning structure, we first consider the motion of a single flux line in the harmonic potential due to the thickness modulation. According to Schmid and Hauger¹⁰ its dynamics are determined by the balance of four different forces: the viscous damping force, the Lorentz driving force, the harmonic pinning force, and the pinning-induced restoring force arising from the interaction with all the other vortices of the lattice. Once the motion of a single vortex line is known, the electrodynamic properties of thickness-modulated layers in the flux-flow regime are easily deduced by averaging the single flux line contributions over the entire vortex lattice.

The equation of motion (per unit length) of a single vortex line l can be written as

$$\eta \vec{v}_l = \eta \dot{\vec{r}}_l = \vec{F}_L - \nabla_l f_l, \quad (44)$$

where \vec{v}_l is the flux-line velocity, $\eta \vec{v}_l$ the viscous damping force, and $\vec{F}_L = (\vec{j} \times \vec{\varphi}_0)/c$ the Lorentz driving force corresponding to a uniform transport current density. The viscosity coefficient η is related to the flux-flow resistivity ρ_f by $\eta = B\varphi_0/c^2\rho_f$. The last term in Eq. (44) is the force arising from the spatial variations of the free energy f_l per vortex line. $\nabla_l f_l$ has been already considered [Eqs. (9) and (19)] in the study of the static interaction of the vortex lattice with the periodic pinning potential and is given by

means of a continuous deformation field $\vec{u}(\vec{r}, \vec{t})$, whereas in our model we shall take into account the discrete nature of the vortex lattice. This is essential in the case of a harmonic pinning potential, where short-wavelength deformations of the vortex lattice play sometimes an important role (Bragg configurations).

We shall now discuss the flux-flow regime in thickness modulated films under various conditions.

B. Matching configurations

Generally, the effect of the pinning forces on a moving vortex lattice results in forced excitation of strongly damped deformation modes of the vortex lattice. A quite different dynamic interaction occurs, however, when the vortex lattice matches a periodic pinning structure. In this case, there is no lattice distortion and each flux line of the moving lattice simultaneously experiences the same pinning potential. In other words, the motion of the whole lattice is the same as that of a single flux line. One is therefore led to imagine a particular flux-flow regime where dynamic coupling of the vortex lattice with the periodic pinning potential gives rise to a highly coherent velocity oscillation of the vortices. This collective oscillation of the flux lines modulates the uniform lattice motion which would exist without pinning.

The equation describing vortex motion in thickness-modulated films assumes a particularly interesting form for matching configurations. Using Eqs. (10) and (13) and the inversion symmetry of the triangular lattice, one can easily verify that the last two terms of $\nabla_{\mathbf{r}} f_i$ in Eq. (45) vanish for an undistorted lattice ($\vec{\mathbf{r}}_{i'} = \vec{\mathbf{r}}_{i'}^0$). From Eqs. (44) and (45) we then deduce the following equation of motion⁷:

$$\eta \dot{\vec{\mathbf{r}}}_i = \vec{\mathbf{F}}_L + \vec{\mathbf{q}} \Delta \epsilon \sin \vec{\mathbf{q}} \cdot (\vec{\mathbf{r}}_i - \vec{\mathbf{r}}_0). \quad (46)$$

The distinctive property of the dynamic matching state is that the oscillating flux-line velocity $\vec{\mathbf{v}}_i(t) = \dot{\vec{\mathbf{r}}}_i(t)$ resulting from Eq. (46) is also the flux-flow velocity $\vec{\mathbf{v}}(t)$ of the whole lattice, i.e., $\vec{\mathbf{v}}(t) = \vec{\mathbf{v}}_i(t)$.

The special interest of Eq. (46) is that it is very similar to that for the time-dependent phase in a resistively shunted Josephson junction, a two-fluid model appropriate for various types of weak links.²³⁻²⁶ As we shall show below, there is, in fact, a strong analogy between flux-flow phenomena in periodic pinning structures and ac Josephson effects²⁷ in arrays of superconducting weak links. In order to specify this point, we consider the fundamental matching configuration $\vec{\mathbf{q}} = \vec{\mathbf{g}}_1$ of Fig. 6, where we assign the role of elementary weak links to regions of the mixed state containing just one of the particular vortex rows drawn in the figure. When the flux-flow regime is driven by a dc transport current, coherent vortex motion in the harmonic pinning potential causes the phase difference θ across an elementary weak link to slip³¹ at an oscillating rate $d\theta/dt = qv(t)$. As a consequence, the voltage²⁷ $V_r(t) = (\hbar/2e)d\theta/dt = \varphi_0 v(t)/c\lambda_g$ appearing across the weak link is also an oscillating function of time. Moreover, the equation governing θ obtained by combining Eq. (46) with $d\theta/dt = qv(t)$ is precisely that of a resistive junction. It appears,

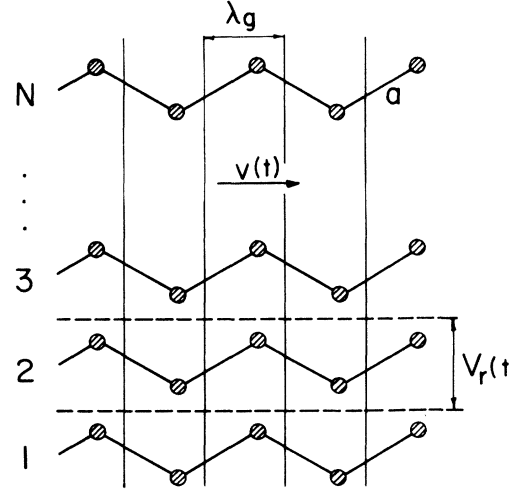


FIG. 6. Vortex rows defining the weak-link oscillators of the matching configuration $\vec{\mathbf{q}} = \vec{\mathbf{g}}_1$ [$a = (2/\sqrt{3})\lambda_g$]. The mixed-state region comprised between the dashed lines represents an elementary weak link. $V_r(t) = \varphi_0 v(t)/c\lambda_g$ is the oscillating voltage across an elementary weak link due to coherent vortex motion in the periodic pinning structure (vertical lines).

therefore, that thickness modulated films in the flux-flow regime are equivalent to series arrays²⁸⁻³⁰ of resistive junction oscillators acting in phase and frequency coherence when the moving vortex lattice matches the harmonic pinning structure (Fig. 6). This means that the oscillating voltage detected across N vortex rows as those shown in Fig. 6 is simply $V(t) = NV_r(t)$, a result characterizing the "superradiant state" in arrays of highly synchronized weak links.²⁸⁻³⁰ Note that the corresponding electric field oscillation $E(t) = V(t)/L$, where L is the distance between the electrodes, obeys the usual flux-flow relation $E(t) = v(t)B_{n_1 n_2}/c$. This can be easily verified by expressing N in terms of L and λ_g (for instance, $N = L\sqrt{3}/2\lambda_g$ for the particular case of Fig. 6) and using Eq. (11).

It is straightforward to extend well-known results of the resistive-junction model to our particular array situation. The oscillating electric field $E(t)$ is given by the following Fourier series solution²⁵ of Eq. (46)

$$\frac{E(t)}{E_{dc}} = 1 + 2 \sum_{m=1}^{\infty} \left(\frac{[1 - (1 - \gamma^2)^{1/2}]^m}{\gamma} \right) \cos m\omega t, \quad (47)$$

where $\gamma = j_{cM}/j_{dc}$ and $\omega = qv_{dc} = cqE_{dc}/B_{n_1 n_2}$ is the fundamental frequency associated with vortex motion in the harmonic pinning structure. $E_{dc} = v_{dc}B_{n_1 n_2}/c$, the time average of $E(t)$, is given by

$$E_{dc} = \rho_f (j_{dc}^2 - j_{cM}^2)^{1/2}. \quad (48)$$

The experimental current-voltage characteristic of thickness-modulated films in the matching state

has been found⁶ in reasonable agreement with Eq. (48).

In a two-fluid model of the flux-flow regime the oscillating electric field given by Eq. (47) is a manifestation of a Josephson-like supercurrent oscillation characterizing the dynamic matching state of thickness-modulated films. The origin of the superfluid oscillation has been discussed in Refs. 7 and 8. It is closely related to the modulating effect of the periodic pinning structure on the oscillating supercurrent density distribution associated with the moving vortex lattice. Since the total dc current carried by the modulated layer is conserved, the voltage oscillation (corresponding to normal fluid) described above is generated across the normal cores of the flux lines by dissipative feedback of the supercurrent oscillation. Note that current conservation is essentially expressed by Eq. (46), where the individual current components of the two-fluid model are easily identified by means of the analogy with the resistively shunted junction.

The fundamental spectral component of $E(t)$ has been recently detected by our group.⁸ ω was typically in the high-frequency to very high-frequency region. The emitted rf power, however, was considerably less than that expected on the basis of a "superradiant" flux-flow state. This is certainly due to partly uncorrelated vortex motion arising from random background pinning in our granular Al films. For instance, if the effect of random pinning results in uncorrelated motion of the N vortex chains defining the weak-link oscillators of our particular array (Fig. 6), the rf power available at the detector input will be proportional to N and not to N^2 as predicted by the superradiant model. In our experiments N was of the order of 10^4 , a value which could reasonably account for the observed rf power reduction.

The response of the moving vortex lattice to an applied electromagnetic field can be described by assuming a driving current density of the form

$$\vec{j}(t) = \vec{j}_{dc} + \vec{j}_{rf} \cos \Omega t. \quad (49)$$

With this expression for $\vec{j}(t)$, Eq. (46) predicts the occurrence of supercurrent steps in the I - V characteristic^{25,26} when the fundamental frequency ω of vortex motion in the harmonic pinning potential is a multiple of Ω ($\omega = n\Omega$), i.e., when

$$E_{dc} = E_n = n\Omega B_{n_1 n_2} / c q. \quad (50)$$

This relation can be also written as $V_{dc} = V_n = n(N\hbar/2e)\Omega$. In this form it clearly shows that thickness-modulated films in the dynamic matching state interact with electromagnetic radiation as macroscopic Josephson junctions quantized in units of $(N\hbar/2e)$. The supercurrent transitions at E_n reflect ac quantum interference³¹ of the natural os-

cillation generated by the moving lattice with the applied rf field. According to Waldram *et al.*,²⁶ subharmonic steps at $E_{mn} = E_n/m$ arising from higher harmonics $m\omega$ of the oscillation [Eq. (47)] should also appear in the I - V curve. These subharmonic structures, however, were found to be inconsistent with analog simulations³² and analytical investigations³³ of Eq. (46). Experimentally, subharmonic transitions have been observed⁷ in the rf excited I - V characteristics of thickness-modulated films. In this connection, however, we point out that the thickness profile of our layers was spatially periodic but not sinusoidal. Accordingly, subharmonic structures could reflect a more general periodic function for the supercurrentlike term appearing in Eq. (46).

The amplitude of the interference steps is an oscillating function of the rf power. At large rf frequencies ($E_1 \gg \rho_f j_{cm}$) the amplitude, Δj_n , of the n th transition is given by^{26,33}

$$\Delta j_n = 2j_{cm} |J_n(E_{rf}/E_1)|, \quad (51)$$

where J_n is a Bessel function of order n and $E_{rf} = \rho_f j_{rf}$. No general analytic expression for Δj_n is available in other limiting cases.

C. Vortex motion at large velocities

To study vortex motion for arbitrary vortex configurations, we have to solve the nonlinear differential Eq. (44). As pointed out by Schmid and Hauger¹⁰ in their study of the random pinning case, an approximate solution of Eq. (44) can be found by considering vortices moving at large velocities ($l \gg l_0$). In this limit the dynamic displacement \vec{u}_i of the vortices from the positions they would assume for flux flow in the absence of pinning is expected to be small, the pinning force being a rapidly oscillating function of time. In this case, a solution of Eq. (44) in powers of the relative thickness modulation $\Delta d/d$ can be obtained using an iterative perturbation method. Generally, this procedure is correct and leads to transparent physical results. In Sec. III.F, however, we shall meet with a particular situation where, even at large flux-flow velocities, our method is no longer valid.

We look for a steady-state solution $\vec{r}_i(t)$ of Eq. (44) of the form

$$\vec{r}_i(t) = \vec{r}_i^0 + \vec{v}_0 t + (\vec{v}_{rf}/\Omega) \sin \Omega t + \vec{u}_i[\vec{r}_i(t), t], \quad (52)$$

where the first three terms on the right-hand side represent the solution of Eq. (44) for the ideal flat-film case ($\nabla_i f_i = 0$) when vortex motion is driven by superimposed dc and rf currents [Eq. (49)]. \vec{v}_0 and \vec{v}_{rf} are therefore related in a simple way to \vec{j}_{dc} and \vec{j}_{rf} , respectively. In the high-velocity limit we assume $u_i \ll \lambda_g$. Taking the derivative of Eq. (52) with respect to time, one obtains for the flux-line vel-

ocity \vec{v}_i

$$\vec{v}_i = \frac{\partial}{\partial t} [\vec{r}_i + (\vec{r}_i \cdot \nabla_i) \vec{u}_i]. \quad (53)$$

The second term on the right-hand side of Eq. (53) is small compared with the first one since $|\nabla_i u_i|$ is at most of the order of $u_i/a \ll 1$. We shall therefore neglect this term in our calculations. The resulting equation of motion for \vec{u}_i will be similar to that derived by Larkin and Ovchinnikov¹⁵ from the microscopic theory but slightly different from that of Schmid and Hauger¹⁰ who have apparently considered the influence of this term on vortex motion. In both cases, however, the general behavior of flux flow in a random pinning structure was found to be independent of the presence or not of $\partial(\vec{r}_i \cdot \nabla) \vec{u}_i / \partial t$. Small differences appear only in the

determination of the width of the interference transitions.

At this stage, in order to keep the calculations within acceptable limits, we introduce a further approximation which consists in ignoring the pinning force arising from the interaction energy variations caused by the periodic film structure. This amounts to neglecting the second term on the right-hand side of Eq. (45). This approximation is mostly justified by the fact that in some important cases we shall discuss later on the contribution of this term to the pinning force is small (nearly matching configurations) or even vanishes (matching and Bragg configurations). Then, by expanding Eqs. (44) and (45) to first order in \vec{u}_i , the following equation of motion for \vec{u}_i is obtained

$$\eta \frac{\partial \vec{u}_i}{\partial t} - 2 \left(\frac{\varphi_0}{4\pi\lambda} \right)^2 \sum_{i'}' \left(f(r_{i'i'}) \vec{u}_{i'} + \frac{\partial f}{\partial r_{i'i'}} (\vec{r}_{i'} \cdot \vec{u}_{i'}) \frac{\vec{r}_{i'i'}}{r_{i'i'}} \right) = -\frac{i}{2} \Delta \epsilon \sum_{\vec{q}, n} (-1)^n \vec{q} (1 + i\vec{q} \cdot \vec{u}_i) J_n(\vec{q} \cdot \vec{v}_{rt}/\Omega) e^{i\vec{q} \cdot (\vec{r}_i - \vec{r}_0)} e^{i(\vec{q} \cdot \vec{v}_0 - n\Omega)t}, \quad (54)$$

where $f(r)$ is the "interaction function" introduced by Fetter and Hohenberg.¹⁸ $f(r)$ is related to the interaction energy $w(r)$ of two flux lines (Sec. II A) by $w(r) = -2(\varphi_0/4\pi\lambda)^2 r f(r)$. In Eq. (54) the sum over the integer n runs from $-\infty$ to $+\infty$ and $\vec{u}_{i'} = \vec{u}_i - \vec{u}_{i'}$.

To solve Eq. (54), we now make use of the fact that at large vortex velocities one expects $\vec{q} \cdot \vec{u}_i \ll 1$. Accordingly, in a first step we may neglect the term proportional to $\vec{q} \cdot \vec{u}_i$ in the expression of the pinning force on the right-hand side of Eq. (54). A solution of the resulting equation accurate to first order in $\Delta d/d$ is of the form

$$\vec{u}_i = \sum_{\vec{q}, n} \vec{u}_n(\vec{q}) e^{i\vec{q} \cdot (\vec{r}_i - \vec{r}_0)} e^{i(\vec{q} \cdot \vec{v}_0 - n\Omega)t}, \quad (55)$$

where the amplitudes $\vec{u}_n(\vec{q})$ are easily determined using the normal coordinate representation of Sec. II D. The resulting expression for \vec{u}_i is then inserted in the pinning force term of Eq. (54) and a new solution, now accurate to second order in $\Delta d/d$, is worked out. Finally, after averaging the single flux-line contributions $\vec{v}_i = \vec{v}_0 + \vec{v}_{rt} \cos \Omega t + \partial \vec{u}_i / \partial t$ over all vortices of the lattice the following expression for the flux-flow velocity $\vec{v}(t)$ is obtained in second-order approximation:

$$\begin{aligned} \vec{v}(t) = & \vec{v}_0 + \vec{v}_{rt} \cos \Omega t + \delta_{\vec{q}, \vec{z}} \left(\frac{\Delta \epsilon}{\eta} \right) \vec{q} \sum_n (-1)^n J_n(z) \sin[(\omega - n\Omega)t - \theta] \\ & - \frac{i}{4} \left(\frac{\Delta \epsilon}{\eta} \right)^2 \sum_{\vec{q}, p} \sum_{mn} \frac{(-1)^{m+n} J_m(z) J_n(z) (\vec{q} \cdot \vec{e}_p)^2 \vec{q}}{D_p(\vec{q}) + i\eta(\omega - m\Omega)} \delta_{2\vec{q}, \vec{z}} e^{i\{[2\omega - (m+n)\Omega]t - 2\theta\}} \\ & + \frac{i}{4} \left(\frac{\Delta \epsilon}{\eta} \right)^2 \sum_{\vec{q}, p} \sum_{mn} \frac{(-1)^{m+n} J_m(z) J_n(z) (\vec{q} \cdot \vec{e}_p)^2 \vec{q}}{D_p(\vec{q}) - i\eta(\omega - m\Omega)} e^{i(m-n)\Omega t}, \end{aligned} \quad (56)$$

where $z = (\vec{q} \cdot \vec{v}_{rt})/\Omega$, $\theta = \vec{q} \cdot \vec{r}_0$, and $\omega = \vec{q} \cdot \vec{v}_{dc}$ is the characteristic frequency for vortex motion in the harmonic pinning structure already found in Eq. (47). Note that in ω the zero-order velocity \vec{v}_0 has been replaced by the actual flux-flow velocity \vec{v}_{dc} . As pointed out by Schmid and Hauger,¹⁰ this improves the quality of the high-velocity approxim-

ation. \vec{v}_{dc} is determined self-consistently from Eq. (56) by averaging $\vec{v}(t)$ with respect to time.

D. Current-voltage characteristics

Let us suppose that there is no applied electromagnetic radiation ($j_{rt} = 0$). Then, by averaging Eq. (56) with respect to time and using the flux-

flow relation $\vec{E} = -(\vec{v} \times \vec{B})/c$ we are led to the following current-voltage characteristic:

$$j_{dc} = (\delta_{\vec{q}, \vec{g}} j_{cM} \sin\theta + \delta_{2\vec{k}, \vec{g}_1} j_{cB} \sin 2\theta) \delta_{E_{dc}, 0} + (E_{dc}/\rho_f) \left[1 + \frac{1}{2} (\rho_f j_{cM})^2 \sum_p (\vec{e}_q \cdot \vec{e}_p)^2 / (E_p^2 + E_{dc}^2) \right], \quad (57)$$

where $E_p = c \rho_f D_p(\vec{k}) / \psi_0 q$. The two Josephson-like terms in Eq. (57) represent the I - V curve at zero voltage for matching ($\vec{q} = \vec{g}$) and Bragg configurations (for convenience in this section we prefer the more specific notation $2\vec{k} = \vec{g}_1$ rather than the $2\vec{q} = \vec{g}$ notation of Sec. II E). When j_{dc} increases, the phase θ automatically adjust itself to give the proper value of j_{dc} until the critical state is reached. One can easily verify that the critical values of θ correspond to the critical r_0 values previously deduced for matching [Eq. (16)] and Bragg configurations [see discussion of Eq. (33)]. Thus, in these two particular cases our model, which was expected to be valid only at large flux-flow velocities, describes remarkably well the static behavior of the vortex lattice in presence of a transport current.

At finite voltages, Eq. (57) is valid only in the high-velocity limit. This clearly results from inspection of the matching case, where the I - V curve obtained by setting $E_p = 0$ in Eq. (57) is nothing but the expansion of the exact matching characteristic [Eq. (48)] for $E_{dc} \gg \rho_f j_{cM}$. For more general situations the shape of the normalized j_{dc}/j_{cM} vs $E_{dc}/\rho_f j_{cM}$ curve depends on the polarization factors $\vec{e}_q \cdot \vec{e}_p$ and the parameters $E_p/\rho_f j_{cM}$ characterizing the lattice configuration under consideration. As far as the E_p 's are concerned, we note that the expression given above can be also written in the form $E_p = B/cq\tau_p(\vec{k})$, where $\tau_p(\vec{k}) = \eta/D_p(\vec{k})$ is the relaxation time associated with viscous damping of the longitudinal ($p=l$) or transverse ($p=t$) deformation modes excited through the dynamic interaction of the moving vortex lattice with the periodic pinning potential.

For some lattice configurations it is possible to carry out a detailed analysis of the current-voltage characteristic. This is the case, for instance, of nearly matching configurations ($|B - B_{n_1 n_2}| \ll B_{n_1 n_2}$), where we know that shear deformations of the vortex lattice predominate (Sec. II F). As a consequence, only the transverse ($p=t$) term of the sum appearing in Eq. (57) needs to be retained in this case. The corresponding polarization factor is given by Eq. (38), whereas the deformation wave vector \vec{k} entering $D_t(\vec{k}) = K_t k^2$ and, hence, E_t is given by Eq. (37). Normalized current-voltage characteristics for nearly matching configurations are shown in Fig. 7 for two values of the ratio $K_t/\Delta\epsilon$ appearing in $E_t/\rho_f j_{cM} = \frac{1}{2}(K_t/\Delta\epsilon)(1-b)^2$. Note that

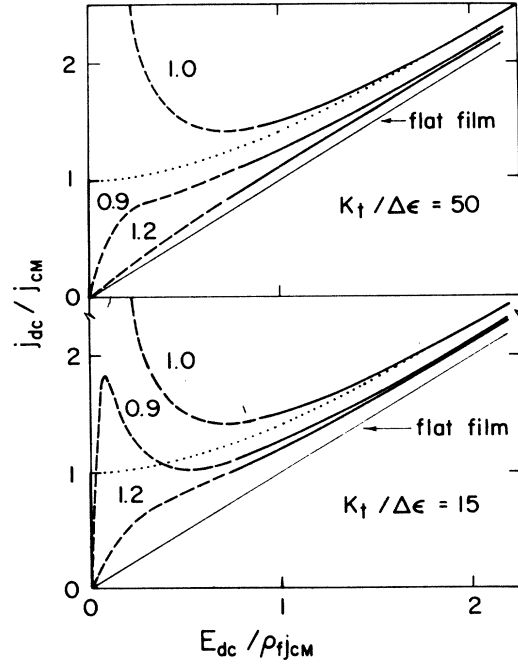


FIG. 7. Normalized flux-flow characteristics of thickness-modulated films near a matching field calculated from Eq. (57). Parameter is the reduced field $b = B_{n_1 n_2} / B$. The dashed portions of the curves approximately show where Eq. (57) is no longer correct. The dotted curve is the exact matching characteristic ($b=1$) deduced from Eq. (48). $K_t/\Delta\epsilon = 15$ is a typical value for the experiments of Ref. 6.

for a given reduced field $b = B_{n_1 n_2} / B$ the shape of the characteristic is more "matchinglike" for the smaller value of $K_t/\Delta\epsilon$. This simply reflects the natural matching tendency of a soft vortex lattice. Figure 7 also shows that our model becomes inaccurate at low flux-flow velocities, where the I - V curves do not extrapolate to finite critical currents and in some cases exhibit a negative dynamic resistance ($dV/dI < 0$) which has not been observed experimentally.⁶ Clearly, a more refined solution of the equation of motion is needed in the low-velocity limit.

At short wavelengths ($ka \sim 1$) dynamic coupling of the vortex lattice with the harmonic pinning structure could also result in the excitation of longitudinal deformation modes. If this is the case, then both terms of the sum in Eq. (57) are generally expected to shape the current-voltage characteristic of Bragg configurations. As noticed in Sec. II E, however, it is possible to separate contributions due to differently polarized modes by selecting Bragg configurations where one of the polarization factors $\vec{e}_q \cdot \vec{e}_p$ vanishes. Note that for Bragg configurations E_t is related to the shear modulus C_{66} of the vortex lattice by Eq. (34).

At a given flux-flow velocity thickness-modulated

films show additional dissipation when compared to a flat reference film. This is due to viscous damping of the lattice deformation modes excited by driven vortex motion in the harmonic pinning potential. The additional time-averaged power dissipation ΔP per unit volume is easily deduced from Eq. (57) and can be written as

$$\Delta P = \frac{1}{2} \rho_f j_{cM}^2 \sum_p (\vec{\epsilon}_q \cdot \vec{\epsilon}_p)^2 \frac{(\omega \tau_p)^2}{1 + (\omega \tau_p)^2}, \quad (58)$$

where $\omega \tau_p = E_{dc}/E_p$. We discuss this expression in the two limiting cases $\omega \tau_p \ll 1$ and $\omega \tau_p \gg 1$. Using the definition $\Delta P = (\eta/A)(\sum_l \overline{u_l^2})_{av}$ (where the subscript *av* denotes a time average) and Eq. (24), one can immediately verify that for $\omega \tau_p \ll 1$ the power dissipation arises from dynamic excitation of the static lattice deformations discussed in Sec. II D. This was expected since in this limit the viscous damping force $\eta \omega u_p(\vec{q})$ in Eq. (54) has negligible influence on vortex motion compared to that of the lattice restoring force $D_p(\vec{k})u_p(\vec{q})$. In contrast, for $\omega \tau_p \gg 1$ the lattice response to the dynamic pinning force becomes unimportant. As a consequence, in this limit Eq. (54) is identical to the equation describing vortex motion at large velocities for a matching configuration. It is therefore not surprising that for $\omega \tau_p \gg 1$ Eq. (58) reduces to ΔP

$$E_{osc}(t) = \frac{1}{2} \rho_f^2 j_{cM}^2 \sum_p (\vec{\epsilon}_q \cdot \vec{\epsilon}_p)^2 \frac{E_p \sin 2(\omega t - \theta) - E_{dc} \cos 2(\omega t - \theta)}{E_p^2 + E_{dc}^2}. \quad (59)$$

Note that $E_{osc}(t)$ has dispersive and absorptive components (proportional to E_p and E_{dc} , respectively) reflecting dynamic excitation of dissipative deformation modes of the vortex lattice similar to that shown in Fig. 3(b). The oscillation has dispersive or absorptive character according to whether $\omega \tau_p \ll 1$ or $\omega \tau_p \gg 1$.

Examination of higher-order terms in the power expansion of $v(t)$ shows that the rf voltage has finite harmonic components also for vortex configurations satisfying the more general condition $m\vec{q} = \vec{g}$ (m integer). For configurations corresponding to a fixed value of m only the $m\omega$ component and its higher harmonics show up in the frequency spectrum of the voltage oscillation. It appears, therefore, that thickness-modulated films in the flux-flow regime are equivalent to current-controlled voltage oscillators whose harmonic content

$\sim \frac{1}{2} \rho_f j_{cM}^2$, the time-averaged power (per unit volume) required to drive the electric field oscillation $E_{osc}(t) = E(t) - E_{dc} \sim \rho_f j_{cM} \cos \omega t$ resulting from Eq. (47) in the corresponding limit $\gamma \ll 1$.

E. Pinning-induced rf oscillations

Here, we are interested in the rf voltage oscillations generated by vortex motion in the periodic pinning structure when the flux-flow regime is driven only by a dc transport current ($j_{rf} = 0$). One can easily verify that for matching configurations the oscillating electric field $E(t) = v(t)B/c$ resulting from Eq. (56) has harmonic components at ω and 2ω with amplitudes equal to the corresponding ones deduced from Eq. (47) in the limit $\gamma \ll 1$. This, of course, is consistent with the assumption of large flux-flow velocities and with the second-order approximation leading to Eq. (56).

According to the present model, when the vortex lattice deviates from a matching configuration the space-averaged rf voltage usually vanishes. For Bragg configurations, however, Eq. (56) predicts the existence of a finite voltage oscillation. In this particular case the oscillating part $E_{osc}(t)$ of the electric field originates from the $\delta_{2\vec{q}, \vec{g}}$ term of Eq. (56) and is given by

can be varied by changing vortex configuration, i.e., by varying B . The amplitude of the spectral components of the oscillation, however, rapidly drops with increasing harmonic order. For this reason only a few of the higher harmonics of the fundamental voltage oscillation might be detected experimentally.

F. Effect of rf radiation

Pinning-induced coupling at rf frequencies causes interference phenomena between the moving vortex lattice and applied electromagnetic fields.^{7,9} Here we study the influence of the interference effect on the current-voltage characteristic when vortex motion is driven by superimposed dc and rf currents [Eq. (49)]. By averaging Eq. (56) with respect to time, after some algebra the following $I - V$ relation is obtained

$$\begin{aligned} j_{dc} = & \rho_f^{-1} E_{dc} + \delta_{\vec{q}, \vec{g}} j_{cM} \sin \theta \sum_n (-1)^n J_n(z) \delta_{E_{dc}, E_n} \\ & + \delta_{2\vec{k}, \vec{g}_1} \frac{1}{2} \rho_f j_{cM}^2 \sin 2\theta \sum_p \sum_{mn} \frac{(-1)^{m+n} J_m(z) J_n(z) (\vec{\epsilon}_q \cdot \vec{\epsilon}_p)^2 E_p}{E_p^2 + \frac{1}{4} (E_m - E_n)^2} \delta_{E_{dc}, (E_m + E_n)/2} \\ & + \frac{1}{2} \rho_f j_{cM}^2 \sum_p \sum_n \frac{J_n^2(z) (\vec{\epsilon}_q \cdot \vec{\epsilon}_p)^2 (E_{dc} - E_n)}{E_p^2 + (E_{dc} - E_n)^2}, \end{aligned} \quad (60)$$

where E_n (and in similar way E_m) is given by

$$E_n = n\Omega B/cq. \quad (61)$$

This expression is a generalization⁷ of Eq. (50) for arbitrary values of B .

Shown in Fig. 8, is the current-voltage characteristic for matching configurations as deduced from Eq. (60). In this case the effect of rf radiation is described by the $\sin\theta$ term and the last term (where $E_p=0$) of Eq. (60). As a result of phase locking³¹ between the fundamental component of the vortex-lattice oscillation and the applied rf field, the Josephson-like term induces sharp supercurrent steps when $E_{dc} = E_n$. One can immediately verify that the magnitude Δj_n of the interference steps is given by Eq. (51), as one expects at large flux-flow velocities and rf frequencies. As shown in Fig. 8, the last term of Eq. (60) modifies the shape of the unexcited characteristic between the interference steps but, unfortunately, diverges for $E_{dc} = E_n$. This shows that for $\tilde{q} \rightarrow \tilde{g}$ the perturbation method used to solve Eq. (54) is no longer valid³⁴ as E_{dc} approaches E_n . Even though this situation is unsatisfactory, we

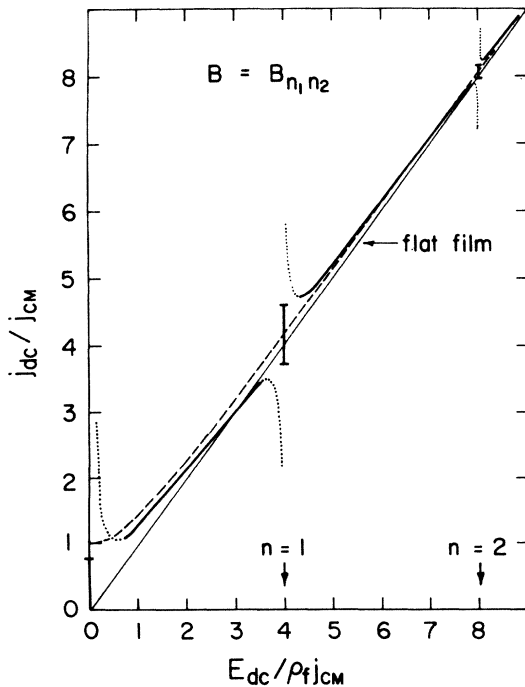


FIG. 8. Effect of rf radiation on the normalized I - V matching characteristic of thickness-modulated films as described by Eq. (60). The supercurrent steps are centered on the unexcited matching characteristic (dashed curve). The dotted branches of the curve show where the second-order perturbation method breaks down. rf frequency and rf power are such that $E_1/\rho_f j_{cM} = 4$ (nearly high-frequency limit) and $E_{rf}/E_1 = z = 1$.

shall not attempt to remove the divergence, as it will not affect the width of the interference transitions in which we are mostly interested here. Note that for $\tilde{q} = \tilde{g}$ our second-order approximation does not predict subharmonic locking, in agreement with the results of Refs. 32–34.

Let us now consider the important case of lattice configurations which slightly deviate from a matching situation ($|B - B_{n_1 n_2}| \ll B_{n_1 n_2}$). In this case, only the transverse ($p=t$) contribution in the last term of Eq. (60) needs to be retained. Since E_t is small, in the high-frequency limit considered here ($E_1 \gg \rho_f j_{cM}$) situations can be easily realized, where $E_1 \gg E_t$ or, equivalently $\Omega\tau_t \gg 1$. It will be subsequently shown that E_t is a measure of the width of the interference transitions. As a consequence, the condition $E_1 \gg E_t$ is just that required to detect distinct interference transitions. Written in the form $\Omega\tau_t \gg 1$ it clearly shows the role of lattice relaxation in quantum interference phenomena of a lattice moving in a harmonic pinning structure. If we now restrict our attention to the portion of I - V curve comprising just a single transition, from Eq. (60) we see that for $\Omega\tau_t \gg 1$ only the corresponding term in the sum over n significantly contributes to j_{dc} . Thus, near E_n we can write

$$j_{dc} \approx \rho_f^{-1} E_{dc} + \frac{1}{2} \rho_f j_{cM}^2 J_n^2(z) (\tilde{\epsilon}_q \cdot \tilde{\epsilon}_t)^2 \times \frac{E_{dc} - E_n}{E_t^2 + (E_{dc} - E_n)^2}, \quad (62)$$

where the polarization factor is given by Eq. (38) and $E_t = (c\rho_f/\varphi_0 q) K_t k^2$ follows from Eq. (37). The divergent behavior found in the matching case ($E_t = 0$) requires a certain precaution in applying Eq. (62). It seems reasonable to assume that the criterion for Eq. (62) to be valid is the absence of regions showing negative dynamic resistance. Elementary algebra shows that this is the case when $J_n(z)\Delta\epsilon < K_t(1-b)^2$. If this condition is satisfied, the current-voltage characteristic has the form shown in Fig. 9. As one can see, dynamic excitation of shear modes of deformation causes broadening of the interference transition at $E_{dc} = E_n$. Using Eq. (37) the transition width ΔE defined in Fig. 9 can be written as

$$\Delta E = 2E_t = (c/\varphi_0)\rho_f K_t q(1-b)^2. \quad (63)$$

This relation, independently of whether the condition $J_n(z)\Delta\epsilon < K_t(1-b)^2$ is fulfilled or not, correctly predicts sharp interference steps for matching configurations ($b=1$). For this reason Eq. (63) is believed to be of general validity as long as $ka \ll 1$, i.e., $|1-b| \ll 1$. Note that on account of the particular nature of vortex motion in a harmonic pinning potential, Eq. (63) is quite different from a corre-

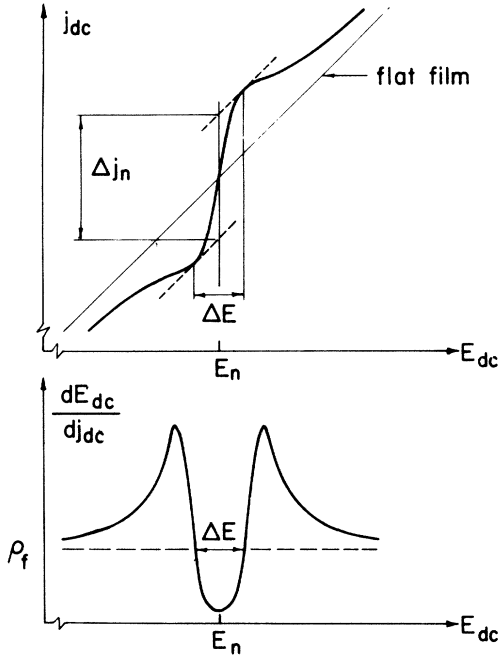


FIG. 9. Rf-induced interference transition in the flux-flow characteristic of thickness-modulated films in a nonmatching state. The I - V curve shown here schematically represents Eq. (62) in the case $J_n(z)\Delta\epsilon < K_t(1-b)^2$. Width ΔE , and height Δj_n , of the transition are given by Eqs. (63) and (64), respectively. The lower part of the figure shows the derivative curve usually measured experimentally.

sponding expression^{10,20,21} for the random pinning case.

Also defined in Fig. 9 is the height Δj_n of the interference transitions. Δj_n can be easily calculated from Eq. (62) and, of course, is found divergent for $b=1$. In order to remove this undesirable feature, we propose the following interpolation formula for Δj_n :

$$\Delta j_n = 2j_{cM} |J_n(z)| \left[1 + \left(\frac{4K_t}{\Delta\epsilon |J_n(z)|} \right) (1-b)^2 \right]^{-1}. \quad (64)$$

This relation reduces to Eq. (51) for $b=1$ and consistently changes into the expression resulting from Eq. (62) when $J_n(z)\Delta\epsilon \ll K_t(1-b)^2$. Note the following interesting property of Eq. (64): when there is no rf excitation, the magnitude of the "zero-order transition" can be written as $\Delta j_0 = 2j_c$, where j_c is given by Eq. (42).

As a final point, we briefly discuss ac quantum interference for Bragg configurations of the vortex lattice. In this case, the $\sin 2\theta$ term of Eq. (60) gives rise to *sharp* interference steps at $E_{dc} = E_n/2$. These subharmonic steps reflect phase locking

between the rf field and the 2ω oscillation of the moving vortex lattice described by Eq. (59). Note that only the dispersive component of Eq. (59) is responsible for the occurrence of these step structures. As it requires the evaluation of a complicated double sum over Bessel function amplitudes, we have not determined their magnitude.

IV. CONCLUSIONS

The model developed in this paper provides, we think, a more than satisfactory description of various phenomena resulting from the interaction of the vortex lattice with a harmonic pinning structure. Although the model has been explicitly worked out for the particular case of superconducting films with harmonically modulated thickness, we feel that it can be extended also to other types of weak periodic pinning structures. We have shown, in fact, that in modulated films the interaction essentially depends on two parameters: the coupling energy $\Delta\epsilon$ associated with the elementary interaction of a single flux line with the pinning potential, and an elastic constant of the vortex lattice describing its response to the harmonic pinning force. In thin films and in the important case of nearly matching configurations, this elastic constant turns out to be the shear modulus C_{66} . Thus, in order to apply the present model to other harmonic pinning structures, one has, in principle, only to determine the basic pinning interaction and to specify the effective elastic constant¹ relevant to the situation under consideration.

Besides describing the electrodynamic properties (critical currents, I - V characteristics, pinning-induced rf voltages, and quantum interference effects) of modulated layers in the matching state, the model also predicts how these properties are modified by the presence of static or dynamic lattice deformations induced by the harmonic pinning force as the vortex lattice deviates from a matching configuration. In this connection, our model suggests the attractive possibility of determining the shear modulus of the vortex lattice from Eq. (42) using a static experimental method or from Eq. (63) using a dynamic technique. For this reason these two relations are considered central results of this paper.

In Sec. III B, we have shown that thickness-modulated films in the dynamic matching state are equivalent to series arrays of resistively shunted Josephson oscillators acting in phase and frequency coherence (superradiant state). This property makes modulated layers potential candidates for device applications as rf detectors and cryogenic voltage oscillators. In this connection, however, we note that a serious limiting factor to

the operation of similar devices is noise generated in real films by random background pinning. The study of this problem undoubtedly requires further theoretical and experimental work.

Several assumptions have been introduced in order to keep the structure of the model as simple as possible. Perhaps, the most serious one is that limiting the description of flux-flow and interference phenomena to large vortex velocities and rf frequencies. Concepts based on the vortex-defect superlattice picture outlined in Sec. II F could prove very useful in determining the nature of vortex motion in the low-velocity limit.

ACKNOWLEDGMENTS

It is a pleasure to thank Professor J. L. Olsen for his enthusiastic interest in this work and for illuminating discussions. I am particularly grateful to Professor J. R. Clem for stimulating suggestions and for elucidating several aspects of this work. Helpful discussions with Dr. A. Baratoff, Dr. A. T. Fiory, Dr. A. F. Hebard, and O. Daldini are also acknowledged. The author would like to thank Professor D. K. Finnemore for the hospitality extended to him during a year's visit to ISU.

*Work performed in part for the Schweizerischer National Fonds zur Förderung der Wissenschaftlichen Forschung and in part for the U. S. ERDA under Contract No. W-7405-Eng-82.

¹A. M. Campbell and J. E. Evetts, *Adv. Phys.* **21**, 199 (1972).

²H. Raffy, J. C. Renard, and E. Guyon, *Solid State Commun.* **11**, 1679 (1972).

³O. Daldini, P. Martinoli, J. L. Olsen, and G. Berner, *Phys. Rev. Lett.* **32**, 218 (1974).

⁴H. Raffy, E. Guyon, and J. C. Renard, *Solid State Commun.* **14**, 427 (1974).

⁵H. Raffy, E. Guyon, and J. C. Renard, *Solid State Commun.* **14**, 431 (1974).

⁶O. Daldini, C. Leemann, and P. Martinoli, *Solid State Commun.* **16**, 509 (1975).

⁷P. Martinoli, O. Daldini, C. Leemann, and E. Stocker, *Solid State Commun.* **17**, 205 (1975).

⁸P. Martinoli, O. Daldini, C. Leemann, and B. van den Brandt, *Phys. Rev. Lett.* **36**, 382 (1976).

⁹A. T. Fiory, *Phys. Rev. Lett.* **27**, 501 (1971).

¹⁰A. Schmid and W. Hauger, *J. Low Temp. Phys.* **11**, 667 (1973).

¹¹P. P. M. Meincke, *Phys. Lett.* **29A**, 208 (1969).

¹²S. Ami and K. Maki, *Prog. Theor. Phys.* **53**, 1 (1975).

¹³L. Dobrosavljević, *J. Phys. (Paris)* **37**, 23 (1976).

¹⁴P. G. de Gennes, *Superconductivity of Metals and Alloys* (Benjamin, New York, 1966), pp. 57-71.

¹⁵A. I. Larkin and Yu. N. Ovchinnikov, *Zh. Eksp. Teor. Fiz.* **65**, 1704 (1973) [*Sov. Phys.-JETP* **38**, 854 (1974)].

¹⁶J. Pearl, *Appl. Phys. Lett.* **5**, 65 (1964); *Proceedings*

of the Ninth Conference on Low Temperature Physics, edited by J. G. Daunt, D. O. Edwards, F. J. Milford, and M. Yaqub (Plenum, New York, 1965), Part A, p. 566.

¹⁷J. R. Clem (private communication).

¹⁸A. L. Fetter and P. C. Hohenberg, *Phys. Rev.* **159**, 330 (1967).

¹⁹E. Conen and A. Schmid, *J. Low Temp. Phys.* **17**, 331 (1974).

²⁰A. T. Fiory, *Phys. Rev. B* **7**, 1881 (1973).

²¹A. T. Fiory, *Phys. Rev. B* **8**, 5039 (1973).

²²I am very grateful to Professor J. R. Clem and Dr. A. Baratoff for many stimulating suggestions and discussions concerning this point.

²³W. C. Steward, *Appl. Phys. Lett.* **12**, 277 (1968).

²⁴D. E. McCumber, *J. Appl. Phys.* **39**, 3113 (1968).

²⁵L. G. Aslamazov and A. I. Larkin, *Zh. Eksp. Teor. Fiz. Pis'ma Red.* **9**, 150 (1968) [*JETP Lett.* **9**, 87 (1969)].

²⁶J. R. Waldram, A. B. Pippard, and J. Clarke, *Philos. Trans. R. Soc. Lond. A* **268**, 265 (1970).

²⁷B. D. Josephson, *Adv. Phys.* **14**, 419 (1965).

²⁸T. D. Clark, *Phys. Rev. B* **8**, 137 (1973).

²⁹D. R. Tilley, *Phys. Lett. A* **33**, 205 (1970).

³⁰D. W. Palmer and J. E. Mercereau, *Appl. Phys. Lett.* **25**, 467 (1974); *IEEE Trans. Mag-11*, 667 (1975).

³¹P. W. Anderson, *Rev. Mod. Phys.* **38**, 298 (1966).

³²P. Russer, *J. Appl. Phys.* **43**, 2008 (1972).

³³M. J. Renne and D. Polder, *Rev. Phys. Appl.* **9**, 25 (1974).

³⁴E. D. Thompson, *J. Appl. Phys.* **44**, 5587 (1973).